The WD and linker domains of ATG16L1 required for non-canonical autophagy limit lethal influenza A virus infection at epithelial surfaces.

Yingxue Wang[†1], Weijiao Zhang[†1], Matthew Jefferson[†1], Parul Sharma[†2], Ben Bone[1], Anja Kipar[2,3], Janine L. Coombes[2], Timothy Pearson[1], Angela Man[4], Alex Zhekova[1], Yongping Bao[1], Ralph A Tripp[5], Simon R. Carding[1,6], Ulrike Mayer[7], Penny P. Powell[1], James P. Stewart[2,5]*& Thomas Wileman[1,6]*

[1]Norwich Medical School, University of East Anglia, Norwich, UK
[2]Department of Infection Biology, University of Liverpool, UK
[3]Institute of Veterinary Pathology, University of Zurich, Switzerland
[4]Earlham Institute, Norwich, UK
[5]Department of Infectious Disease, University of Georgia, Georgia, USA
[6]Quadram Institute Bioscience, Norwich, UK
[7]School of Biological Sciences, University of East Anglia, Norwich, UK

*Corresponding authors: E. mail: t.wileman@uea.ac.uk, j.p.stewart@liv.ac.uk
[†]These authors contributed equally to this work

Summary

Phagocytosis and autophagy represent two evolutionarily ancient pathways that provide an important defense against infection by delivering pathogens to lysosomes for degradation. Phagocytosis and autophagy are linked by non-canonical autophagy pathways that conjugate LC3 to endo-lysosome compartments to facilitate phagosome maturation and lysosome fusion. A role for non-canonical autophagy in host defence is implied from cellular studies *in vitro*, but critically, these studies have rarely been extended to infection of model organisms with intact epithelial barriers and complex immune systems. To address this, we developed a mouse model with specific loss of non-canonical autophagy by removing the WD and linker domain of ATG16L1 required for recruitment of LC3 to endo-lysosome compartments. The mice retain the coiled-coiled domain of ATG16L1 required for conventional autophagy and maintain tissue and immunological homeostasis. Mice with systemic loss of non-canonical autophagy are exquisitely sensitive to low-pathogenicity murine-adapted influenza A virus leading to extensive viral replication throughout the lungs, cytokine dysregulation, fulminant pneumonia and lung inflammation leading to high mortality associated with virulent strains. Conditional mouse models and *ex vivo* analysis showed that protection against IAV infection of lung required non-canonical autophagy within epithelial barriers but was independent of phagocytes and other leukocytes. This establishes non-canonical autophagy pathways in epithelial cells as a novel innate defence mechanism that can restrict IAV infection at mucosal surfaces.

Introduction

Phagocytosis and autophagy provide two evolutionarily ancient and complimentary pathways to transport microbes to lysosomes where they are killed and degraded. Phagocytosis is directed at extracellular organisms entering cells in endocytic vacuoles resulting in the formation of phagosomes that fuse with lysosomes. In contrast, macroautophagy (hereafter called autophagy), is directed at intracellular pathogens and uses autophagosomes to deliver microbes directly to lysosomes. In both cases degradation in lysosomes releases microbial components to alert innate and acquired immune responses. Recent work shows that autophagy and phagocytosis can be linked by non-canonical autophagy. This is best characterized in phagocytic cells where LC3 associated phagocytosis (LAP) is activated by Toll-like receptor signaling resulting in recruitment of autophagy marker protein LC3 to the phagosome membrane to enhance phagosome maturation [1-5]. In non-phagocytes a similar non-canonical pathway recruits LC3 to endo-lysosome compartments during the uptake of particulate material such as apoptotic cells and aggregated β-amyloid and following membrane damage during pathogen entry or osmotic imbalance induced by lysosomotropic drugs [6,7] [8-10]. LC3 can be recruited to endo-lysosome compartments during the uptake of pathogens and extracellular material, but the roles played by non-canonical autophagy during infection *in vivo* are largely unknown. It is not known for example, if non-canonical autophagy is important in the control of infection by epithelial cells at sites of infection, or if it plays a predominant role within phagocytes and antigen-presenting cells.

At present a role for non-canonical autophagy in host defence has been implied from *in vitro* studies of LAP in phagocytes and microbes with a tropism for macrophages such as *Listeria monocytogenes* [11], *Legionella dumoffii* [12], *Leishmania major* and *Aspergillus fumigatus* [13-15]. Critically, these studies have rarely been extended to model organisms with intact epithelial barriers and complex immune systems. An understanding of the roles played by non-canonical autophagy *in vivo* has been hampered because of a lack animal models able to dissect closely interlinked conventional and non-canonical autophagy pathways (Fig.1). Deletion of genes required for conventional autophagy results in neonatal lethality. Mice with tissue-specific loss of *Atg3, Atg5, Atg7, Atg12 and Atg16L1* survive, but the targeted tissues harbor pro-inflammatory macrophages [16,17], show signs of inflammation and tissue damage, and is not possible to determine if any altered phenotype results from loss of autophagy or non-canonical autophagy. Rubicon stabilises the PHOX:NOX2 complex [18] allowing reactive oxygen species (ROS) to induce binding of ATG16L1 to endo-lysosome membranes [4]. The key role played by Rubicon prompted Martinez *et al*. to generate Rubicon$^{-/-}$ mice. These mice have loss of non-canonical autophagy [4] but are difficult to use in infection studies because Rubicon has activities within the immune system that are functionally and genetically separate from effects on non-canonical autophagy, including suppression of NFκB signaling and pro-inflammatory responses [19]. In addition, Rubicon$^{-/-}$ mice fail to gain weight, and have defects in the clearance of dying and apoptotic cells that eventually lead to autoimmune disease that resembles systemic lupus erythematosus [20]. Similarly, deletion of Nox2 has been used to study LAP during Listeria infection [11] but Nox2 mice have combined loss of

ROS and LAP making it difficult to dissect the specific roles played by the inherent antimicrobial activity of ROS and LAP during infection *in vivo*.

We have taken the alternative approach of targeting events downstream of Nox2 and Rubicon to avoid anomalies within the immune system. Fig. 1 shows that the key difference between autophagy and non-canonical autophagy is the use of the WD domain of ATG16L1 to recruit the ATG16L1:ATG5-ATG12 complex to endo-lysosome or vacuole membranes. We have shown that the WD domain of ATG16L1 is required for LAP during uptake of yeast *in vitro* and for non-canonical conjugation of LC3 to endo-lysosome membranes following osmotic imbalance induced by lysosomotropic drugs [2]. This prompted us to generate a mouse lacking the WD domain of ATG16L1 to study the role played by non-canonical autophagy *in vivo* [21]. The mouse model (δWD [Atg16L1$^{\delta wd/\delta wd}$]) carries a stop codon after the coiled coil domain which removes amino acid residues at 266 and 319 in the linker region and conserved phenylalanine residues at positions 467 and 490 in the WD domain required for lipid binding of ATG16L1 and subsequent recruitment of ATG5-ATG12 to endo-lysosome membranes [2,22]. As a consequence the mice are unable to conjugate LC3 to endo-lysosome membrane compartments [21], but the mutation preserves the N-terminal ATG5-binding domain and glutamates at positions 226 and 230 in the CCD of ATG16L1 that are required for WIPI2 binding and autophagy [23]. Importantly, and unlike other mouse models of non-canonical autophagy [4,20], the mice grow normally, do not have pro-inflammatory phenotype and maintain tissue homeostasis [21].

Influenza A virus (IAV) is a negative-strand RNA virus that is a respiratory pathogen of major global public health concern, causing seasonal outbreaks in human populations [24]. Animal reservoirs can contribute to zoonotic infection leading to pandemics with a high incidence of viral pneumonia, morbidity and mortality. The increasing risk of an influenza pandemic emphasizes the need to understand better IAV-host interactions. Infection of the lower respiratory tract of can result in flooding of alveolar spaces, acute respiratory distress syndrome and respiratory failure leading to death. IAV infects airway and alveolar epithelium and damage results from a combination of the intrinsic pathogenicity of individual virus strains as well as the strength and timing of the host innate/inflammatory responses. Optimal cytokine levels protect from IAV replication and disease but excessive cytokine production and inflammation worsens the severity of lung injury [25-29]. Infection and entry of IAV into cells involves viral attachment, via the hemagglutinin (HA) glycoprotein that is embedded in the virion membrane, to cell surface receptors that contain sialic acid [30]. After binding, virus particles enter the cell by receptor-mediated endocytosis. Acidification of late endosomes causes a structural change in HA resulting in fusion with the endosomal membrane and delivery of viral ribonuclear proteins (RNPs) into the cytoplasm [30,31]. RNPs are then imported into the nucleus, where genome replication and transcription of viral genes take place [32].

It is known that IAV induces non-canonical autophagy during infection *in vitro* [2]. However, the role played by non-canonical autophagy in defending against IAV infection *in vivo* is currently unknown. Herein we elucidate for the first time the function of non-canonical autophagy in host defence to IAV in the whole organism. We used a low-pathogenicity murine-adapted IAV (A/X-31) that does not normally lead to extensive viral replication throughout the lungs, or cause the cytokine dysregulation and death typically seen after infection with highly pathogenic viral strains [33] We show that loss of the WD and linker domain of ATG16L1 from all tissues renders mice highly sensitive to influenza virus A (IAV). Use of conditional mouse models showed that protection against virus (IAV) infection of lung was dependent on the presence of the WD and linker domains of ATG16L1 within epithelial barriers, rather than in phagocytes or other immune cells. This establishes non-canonical autophagy pathways in epithelial cells as a novel innate defence mechanism that restrict IAV infection at mucosal surfaces.

Results

Mice with systemic loss of the WD and linker domains of ATG16L1 are highly sensitive to IAV infection

The consequences of loss of the WD and linker domains of ATG16L1 on conventional autophagy and non-canonical autophagy were confirmed using cell lines taken from controls and δWD mice. Mouse embryo fibroblasts (MEFs) from littermate control mice expressed full-length α and β forms of ATG16L1 at 70kDa (Fig. 1B), and generated PE-conjugated LC3II during recruitment of LC3 to autophagosomes following starvation in HBSS. The MEFs also recruited LC3 to endo-lysosome compartments swollen by monensin. Bone marrow-derived macrophages (BMDM) from the control mice also activated LAP to recruit LC3 to phagosomes containing zymosan. MEFs from δWD mice expressed a truncated ATG16L1 at 30 kDa (Fig. 1C). Cells from δWD mice generated LC3II and autophagosomes in response to starvation, but failed to recruit LC3 to swollen endo-lysosome compartments or phagosomes containing zymosan. These data confirm the indicated selective defects in non-canonical autophagy and LAP in the δWD mice.

IAV enters airway and lung epithelial cells by endocytosis, and in tissue culture IAV induces non-canonical autophagy leading to ATG16L1-WD domain-dependent conjugation of LC3 to the plasma membrane and peri-nuclear structures [2]. To test whether non-canonical autophagy has a host defence function in the host *in vivo*, δWD mice were infected with IAV. We used a low-pathogenicity murine-adapted IAV (A/X31) that does not normally lead to extensive viral replication throughout the lungs, or cause the cytokine storm and death typically seen after infection with highly pathogenic viral strains. The results (Fig. 2) showed that δWD mice became moribund and showed severe signs of clinical illness (rapid breathing, piloerection). They also displayed rapid weight loss compared to littermate controls (Fig. 2A) and had increased mortality with survivors recovering more slowly from infection (Fig. 2B). The increased weight loss was associated with an approx. log increase in lung virus titre at 5 days post-infection (d.p.i.; Fig. 2C). Furthermore, histopathology and immunohistochemistry (IH) analysis of lungs from δWD mice showed fulminant viral pneumonia with large numbers of IAV-positive cells (Fig. 2D).

The WD and linker domains of ATG16L1 required for non-canonical autophagy control lung inflammation after IAV infection

Innate protection against IAV is provided by type 1 (α, β) and III (λ) interferon (IFN) with severe IAV infection causing excessive airway inflammation and pulmonary pathology attributable in part to IFNαβ and TNF-α [27,34]. Measurement of cytokine expression at 2 d.p.i showed that IAV induced a transient increase in transcripts for interferon-stimulated genes (ISGs), ISG15 and IFIT1 [28] and pro-inflammatory cytokines

(IL-1β, TNF-α, and CCL2 [MCP-1]) in the lungs of both control and δWD mice (Fig. 3A). In control mice the increased cytokine expression was resolved by 3 d.p.i, but δWD mice showed sustained increases in IL-1β, TNF-α and CCL2 transcripts, co-incident with exacerbated weight loss. Lungs of δWD mice showed increased expression of neutrophil chemotaxis factor CXCL1 mRNA (Fig. 3A), coincident with increased neutrophil infiltration of airways and parenchyma, and extensive neutrophil extracellular traps (NETs) as a consequence of neutrophil degeneration as shown by IH (Fig. 3B and S1). Increased neutrophil infiltration of airways in δWD mice at 2 d.p.i. was confirmed and quantified using flow cytometric analysis of broncho-alveolar lavage (BAL; Fig. 3C). At 5 - 7 d.p.i. Increased expression of CCL2 mRNA in δWD mice was coincident with extensive macrophage/monocyte infiltration into lung parenchyma observed by IH (Fig. 3B and S2) which was not seen in controls. This increased macrophage/monocyte infiltration in δWD mice was confirmed and quantified using flow cytometric analysis of lung tissue (Fig. 3C). It is known that, in severe IAV infection, a cytokine storm occurs that is amplified by plasmacytoid dendritic cells pDCs [27]. pDCs detect virus-infected cells and produce large amounts of cytokines, in particular IFNαβ, that in severe infections can enhance disease. In these cases, depletion of pDCs can decrease morbidity [27]. Depletion of pDCs in IAV-infected δWD mice using anti-PDCA-1 led to markedly decreased weight loss as compared with isotype control-treated mice and that was similar to that seen in littermate controls. This indicates that excessive cytokine production amplified by pDCs is responsible for the increased morbidity seen in the δWD mice.

Thus, mice with systemic loss of non-canonical autophagy failed to control lung virus replication and inflammation, leading to increased cytokine production, morbidity and mortality.

Systemic loss of the WD and linker domains of ATG16L1 does not lead to gross changes in inflammatory threshold or immunological homeostasis

Macrophages cultured from mice with complete loss of ATG16L1 secrete high levels of IL1-β [17], and LysMcre-mediated deletion of genes essential for conventional autophagy (eg: Atg5, Atg7, Atg14, Atg16L1, FIP200) in mice leads to raised pro-inflammatory cytokine expression in the lung, and increased resistance to IAV infection [Fig. S3 and [16]]. This led us to test the possibility that the δWD mutation could also increase IL-1β secretion, and cause the increased inflammation observed during IAV infection. This was tested by incubating BMDM with LPS and purine receptor agonist, BzATP (Fig S4A), or by challenging mice with LPS (Fig S4B). Mice with a complete loss of ATG16L1 in myeloid cells (Atg16L1$^{fl/fl}$-lysMcre) showed three-fold increases in IL-1β in serum and secretion of secretion IL-1β from BMDM *in vitro*. In contrast IL-1β secretion in δWD mice did not differ significantly from littermate controls. This was consistent with lack of elevated cytokines in lungs prior to infection (see day 0 in Fig. 3A), and our previous work showing that serum levels of IL-1β, IL-12p70, IL-13, and TNF-α in δWD mice are the same as in littermate controls at 8-12 and 20-24 weeks [21]. The exaggerated inflammatory response to IAV did not therefore result from a raised pro-inflammatory threshold or dysregulated IL-1β responses in the lung. Also, the frequencies of T-cell, B-cell and macrophages were similar in δWD mice to littermate controls (Fig. S5). These data suggest that the exaggerated responses of δWD mice to IAV do not occur because the mice have a raised inflammatory threshold or abnormal immunological homeostasis.

The WD domain and linker domains of ATG16L1 limit IAV infection independently of phagocytic cells

The link between non-canonical autophagy/LAP, TLR signalling, NADPH oxidase activation and ROS production [1,4,5] provides phagocytes with a powerful mechanism to limit infections *in vivo*. To test whether wild-type bone marrow-derived cells could protect susceptible δWD mice from lethal IAV infection, we generated radiation chimeras (Fig. S6). When challenged with IAV, δWD mice reconstituted with either wild-type or δWD bone marrow remained highly sensitive to IAV (Fig. 4A & B) with body weight reduced by up to 25% and decreased survival by 5 d.p.i. As seen for δWD mice, weight loss was associated with a 10-fold increase in lung viral titre (Fig. 4C), fulminant pneumonia and inflammatory infiltration into the lung (Fig. 4D). This increased susceptibility to IAV was not observed for control mice reconstituted with wild-type marrow, showing that non-canonical autophagy pathways in phagocytes and other leukocytes from control mice were not able to protect δWD mice against lethal IAV infection. In a reciprocal experiment (Fig. S7) mice expressing cre recombinase in myeloid cells (LysMcre) were used to generate mice (called $\delta\text{WD}^{\text{phag}}$), where the truncated *Atg16*L1δWD gene was restricted to phagocytic cells. In these mice, non-canonical autophagy was absent in cultured phagocytes (BMDM) but it was present in skin fibroblasts (Fig S7D). After infection with IAV, $\delta\text{WD}^{\text{phag}}$ mice showed comparable weight loss and virus titres to those seen in littermate control mice (Fig. 5A & B). Likewise, the raised IL-1β levels (Fig. 5C) and profuse macrophage and neutrophil lung infiltration observed in δWD mice was absent (Fig. S8) and similar to littermate controls. Thus, the sensitivity of δWD mice to IAV was not due to the loss of non-canonical autophagy from myeloid cells, making it likely that the activity of the WD and linker domains of ATG16L1 protect against lethal IAV infection in non-myeloid tissue. The ability of the WD and linker domains of ATG16L1 to protect epithelial cells against IAV infection was tested *ex vivo* to further exclude any contribution from recruited leukocytes. Virus titres in precision cut lung slices (Fig. 5D) from δWD mice were 10-fold greater than controls. The activation of interferon responses following IAV infection in non-phagoyctic cells was also confirmed. MEFs from δWD mice showed between 3 and 5-fold increases in expression of IFN responsive genes, ISG15 and IFIT1 (Fig. 5E & F), and this was also observed in the lung *in vivo* (Fig. 3A).

Taken together the results demonstrate for the first time that the WD and linker domains of ATG16L1 allow non-canonical autophagy to provide a novel innate defence mechanism against lethal IAV infection within the epithelial barrier *in vivo*.

Discussion

We have generated a mouse model δWD) to study the role played by non-canonical autophagy during infection *in vivo*. The δWD mice lacking the WD and linker domains of ATG16L1 grow normally, have normal levels of autophagy, and therefore maintain tissue homeostasis [21]. Importantly, δWD mice do not have a pro-inflammatory phenotype seen following loss of autophagy from myeloid cells [16,17] or systemic loss of Rubicon [20]. δWD mice showed profound sensitivity to infection by a low-pathogenicity murine-adapted IAV (A/X31). In contrast to control mice, there was extensive viral replication throughout the lungs, cytokine dysregulation, fulminant pneumonia and lung inflammation leading to high mortality and death only usually seen after infection with virulent strains [33]. These signs mirror the cytokine storms and mortality seen in humans infected with highly pathogenic strains of IAV such as the 1918 ‘Spanish’ Influenza [33].

The observation that bone marrow transfers from wild-type mice were unable to protect δWD mice from IAV suggested that protection against IAV infection *in vivo* was independent of leukocytes and did not require non-canonical autophagy in leukocyte populations (e.g. macrophages, dendritic cells, neutrophils, granulocytes, lymphocytes). In a reciprocal experiment the linker and WD domains of ATG16L1 were deleted specifically from myeloid cells. These mice, which lack non-canonical autophagy in phagocytic cells (LAP), but maintain non-canonical autophagy in other tissues, failed to show increased sensitivity to IAV infection. Thus, protection against severe IAV-associated disease in the host relies heavily on non-canonical autophagy in non-leukocyte populations.

Activation of non-canonical autophagy in phagocytic cells leads to LC3 associated phagocytosis (LAP) where TLR signalling and reactive oxygen species (ROS) recruit LC3 to phagosomes. A lack of involvement of LAP in protection against IAV disease *in vivo* was surprising because the activation of LAP in phagocytic cells such as macrophages, dendritic cells and neutrophils by would provide a powerful means of recognising and controlling microbial infection *in vivo*. *In vitro* studies show that activation of acid sphingomyelinase by *Listeria monocytogenes* [11] and subsequent ROS production by NOX2 recruit LC3 to phagosomes. Similarly, activation of TLR2 and NOX2 by *Legionella dumoffii in vitro* signal ULK1-independent translocation of LC3 to single-membraned vacuoles containing Legionella [12]. In both cases LC3 promotes fusion with lysosomes. The observation that virulence factors such as the GP63 metalloprotease of *Leishmania major* and melanin of *Aspergillus fumigatus* prevent recruitment of NOX2 to phagosomes to prevent LAP [13-15] further suggest that non-canonical autophagy in phagocytes should provide a defence against infection. One reason for the discrepancy may be that the studies cited above have focused on *in vitro* experiments using microbes with a tropism for macrophages, rather than *in vivo* studies where pathogens encounter epithelial barriers.

Intranasal infection of mice with IAV results in rapid infection of principally airway and pulmonary epithelial cells [35]. The results of *in vivo* challenge of radiation chimaeras and δWD^{phag} mice strongly suggest that non-canonical autophagy in the epithelium rather than leucocytes is responsible for restricting IAV infection. This was supported by *ex vivo* experiments where virus titres and interferon responses were 5 - 10 fold greater in precision-cut lung slices and MEFs from δWD mice. Non-canonical autophagy in epithelial cells may reduce IAV replication by increasing transfer of endocytosed virus to lysosomes for degradation. This may involve increased fusion with lysosomes following recruitment of LC3 by TMEM59 [36], or by maintaining membrane repair during virus entry, as observed for *S*. Typhimurium and *Listeria monocytogenes* [7,37]. A p22^{phox}-NOX2 pathway that recruits LC3 to vacuoles containing *S*. Typhimuriumin epithelial cells [38] may also be activated during IAV entry and hamper lethal infection.

δWD mice infected with IAV appeared to be unable to resolve inflammatory responses resulting in sustained expression of pro-inflammatory cytokines, morbidity and a striking lung pathology characterized by profuse migration of neutrophils into the airway at day 3 followed by macrophages on day 7. pDCs detect IAV-infected cells and produce large amounts of cytokines, in particular IFNαβ, that in severe infections can enhance disease[27]. The fact that morbidity in δWD mice could be decreased by depleting pDCs indicates that excessive cytokine production, amplified by pDCs was a major factor. This is not due to a lack of non-canonical autophagy/LAP in pDC as bone-marrow chimaeras of δWD mice with wild-type leukocytes have the same phenotype as δWD mice. IAV is recognized by endosomal TLR3 in respiratory epithelial cells and RIG-I detects virus replicating in the cytosol leading to activation of IRF3 and NFkB with subsequent induction of interferon, ISG and proinflammatory cytokine production [28]. Increased inflammation may result directly from increased virus in the lungs, but it is possible that delivery of IAV from endosomes to lysosomes is reduced in the airway epithelial cells of δWD mice resulting in the sustained TLR3 and pro-inflammatory cytokine signalling. A similar pro-inflammatory phenotype resulting from decreased trafficking of inflammatory cargoes is observed following disruption of non-canonical autophagy by LysMcre-mediated loss of Rubicon from macrophages or microglia [6,20].

We have approached the problem of dissecting the roles played by conventional autophagy and non-canonical autophagy *in vivo* by removing the linker and WD domain from ATG16L1 to prevent conjugation of LC3 to single-membraned endo-lysosome compartments [21]. An alternative approach has been to target pathways upstream of LC3 conjugation. Tissue-specific loss of components of the ULK1 complex (eg: ULK1, FIP200 or ATG13) can remove autophagy without affecting non-canonical autophagy [4,39]. Similarly, deletion of Rubicon produces a selective block in LAP [4,6]. Mouse models relying on loss of Rubicon show defects in the clearance of bacterial and fungal pathogens and apoptotic cells [4,20], but unlike our study disruption of Rubicon also leads to upregulation of IL-1β, IL6 and TNF-α secretion, and the mice develop an autoimmune disease that resembles Systemic Lupus Erythematosus [20,40]. This exaggerated inflammation makes it difficult to determine if changed responses to infection *in vivo* result from loss of non-canonical autophagy or from upstream changes in cytokine regulation.

Several non-canonical pathways leading to recruitment of LC3 to endo-lysosomal compartments, rather than phagosomes, are beginning to emerge. Non-canonical autophagy in microglia facilitates endocytosis of β–amyloid and TLR receptors to reduce β-amyloid deposition and inflammation in mouse models of Alzheimer's disease [6]. This may involve and interaction between the WD domain and TMEM59 which is required for β-amyloid glycosylation [41]. Lysosomotropic drugs, which stimulate direct recruitment of LC3 to endosomes, create pH and osmotic changes that may mimic the consequences of viral infections that perturb endosome membranes or deliver viroporins to endo-lysosome compartments. It will be interesting to see if the WD and linker domains of ATG16L1 limit infection by other microbes at epithelial barriers *in vivo*. This may be true for picornaviruses where LC3 is recruited to enlarged endosomes during entry of Foot and Mouth Disease virus [42] and following LC3 accumulation on megaphagosomes in pancreatic acinar cells during coxsackievirus B3 infection [43]. In the specific case of IAV, non-canonical autophagy mediated by non-canonical autophagy at epithelial barriers is likely important for innate control of new pathogenic strains, where acquired immunity from previous infection may be absent or less effective. It will be valuable to assess whether human allelic variants of ATG16L1 confer altered resistance/susceptibility to IAV and whether drug-based manipulation of non-canonical autophagy can increase resistance at the epithelial barrier.

Acknowledgements

This work was funded in part by Biotechnology and Biological Sciences Research Council (BBSRC) grant BB/R00904X/1 to JPS, JLC SRC, PPP, UM and TW, and through BBSRC Institute Strategic Programme Gut Microbes and Health BB/R012490/1: BBS/E/F/000PR10353, BBS/E/F/000PR10355

Author contributions

TW, JPS, PPP, SRC and JLC conceived the experiments. Mouse strains were generated by UM and genotyped by MJ, SR and WZ. Immunological homeostasis was assessed by WZ, AM and AZ. Animal infections were carried out by JPS, YW, WZ, and PS and histology and immunohistology by AK. Downstream analysis was performed by YW, WZ, PS, TP and PPP. *In-vitro* analysis was performed by BB, TP and PPP. The manuscript was drafted by TW, JPS, YB, PPP, RAT and UM and edited and approved by all authors

Declaration of interests: Authors declare no competing interests.

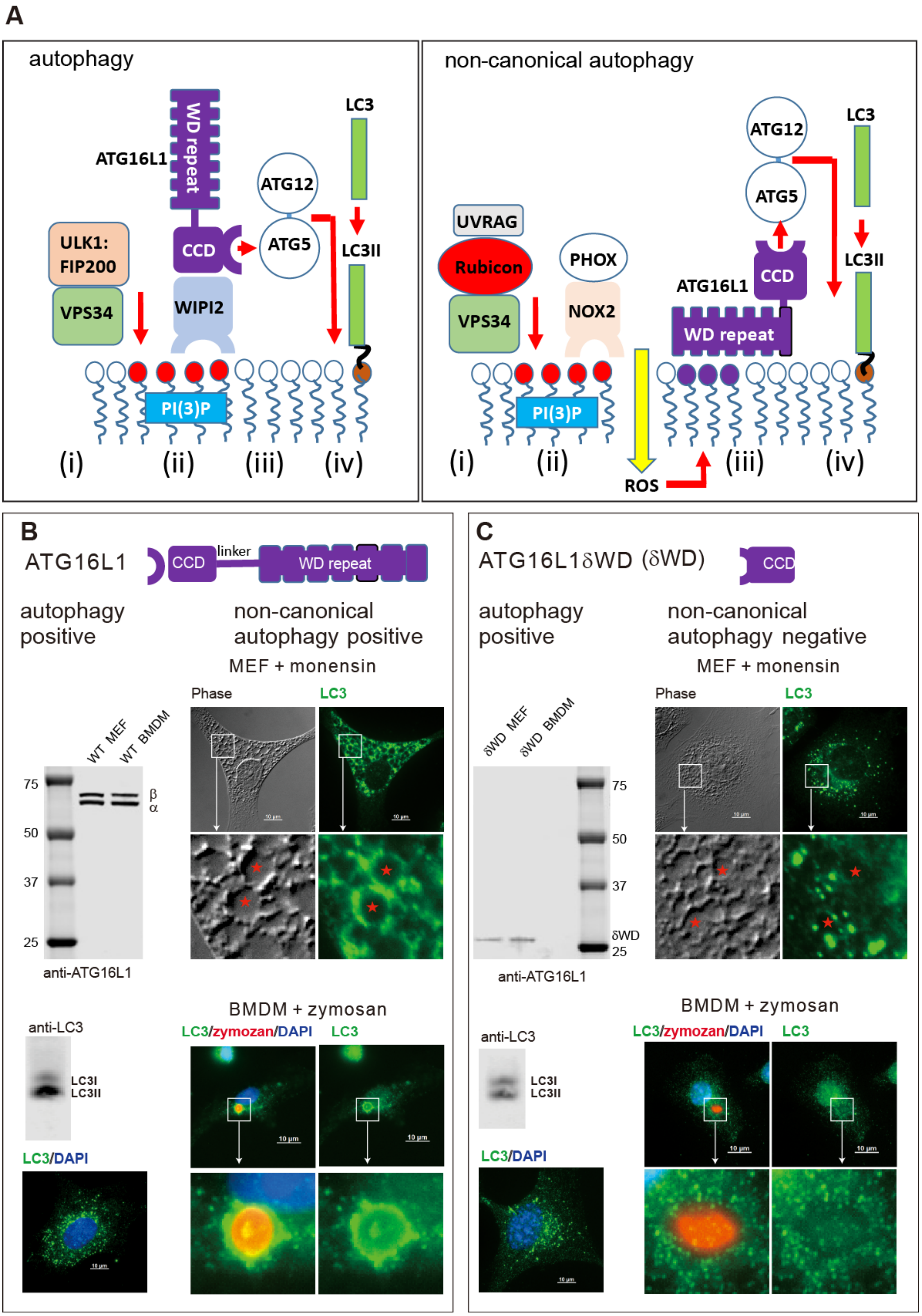
A
autophagy
ATG16L1
WD repeat
ULK1:
FIP200
VPS34
CCD
WIPI2
ATG12
ATG5
LC3
LC3II
PI(3)P
(i)
(ii)
(iii)
(iv)
non-canonical autophagy
UVRAG
Rubicon
VPS34
PHOX
NOX2
ATG12
ATG5
CCD
ATG16L1
WD repeat
LC3
LC3II
PI(3)P
ROS
(i)
(ii)
(iii)
(iv)
B
ATG16L1
CCD
linker
WD repeat
autophagy positive
non-canonical autophagy positive
MEF + monensin
Phase
LC3
WT MEF
WT BMDM
75
50
37
25
β
α
anti-ATG16L1
10 μm
BMDM + zymosan
anti-LC3
LC3I
LC3II
LC3/zymozan/DAPI
LC3
LC3/DAPI
C
ATG16L1δWD (δWD)
CCD
autophagy positive
non-canonical autophagy negative
MEF + monensin
Phase
LC3
δWD MEF
δWD BMDM
75
50
37
δWD
25
anti-ATG16L1
BMDM + zymosan
anti-LC3
LC3I
LC3II
LC3/zymozan/DAPI
LC3
LC3/DAPI
10 μm

Fig. 1. Deletion of the WD domain of ATG16L1 causes loss of non-canonical autophagy and LAP but retains autophagy.

A). Conventional autophagy is activated by the initiation complex containing ULK1, FIP200 and the PI3 kinase VPS34 (i) which responds to starvation. The VPS34 subunit phosphorylates lipids in membranes to generate sites for WIP2 binding (ii). WIPI2 binds the coiled coil domain (CCD) of ATG16L1 (ii) leading to recruitment of ATG16L1 and the LC3 conjugation machinery (ATG16l1:ATG5-ATG12, ATG7, ATG3) (iii). This results in conjugation of LC3 to PE in the surface of the autophagosome (iv) to promote fusion with lysosomes.

During non-canonical autophagy signalling pathways arising from the lumen of the endosome or phagosome recruit a complex containing UVRAG, Rubicon and VPS34 (i). The VPS34 subunit phosphorylates lipids in endo-lysosome membranes to generate sites for binding the multicomponent PHOX:NOX2 complex (ii) which is stabilised by Rubicon to generate reactive oxygen species (ROS). ROS induces binding of the WD domain of ATG16L1 to endo-lysosome membranes (iii) leading to recruitment of the LC3 conjugation machinery (ATG16l1:ATG5-ATG12, ATG7, ATG3) (iii) and conjugation of LC3 to PE (iv)

B) Left column: MEFs from littermate control express α and β isoforms of ATG16L1 at 70 kDa, convert LC3I to LC3II and generate LC3 puncta during autophagy induced by HBSS. **Right column:** LC3 (green) is recruited to endo-lysosomes following induction of non-canonical autophagy by monensin, and to phagosomes following engulfment of zymosan by bone marrow-derived macrophages (BMDM).

C) Left column: MEFs from δWD mice express a 30kDa truncated ATG16L1, but still convert LC3I to LC3II and generate LC3 puncta following autophagy induced by HBSS. **Right column:** The δWD MEFs do not recruit LC3 (green) to endo-lysosomes following incubation with monensin or to bone marrow-derived macrophage phagosomes containing zymosan**.**

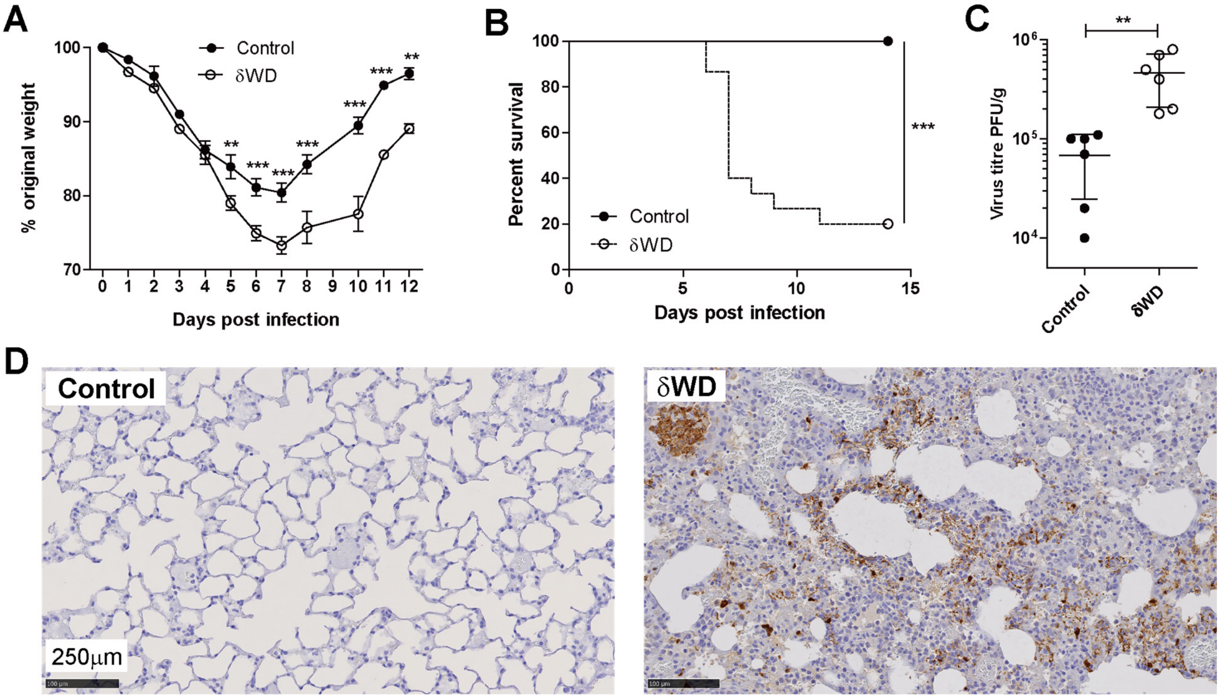

Fig. 2. Systemic loss of non-canonical autophagy increases susceptibility to IAV infection. Littermate control and δWD mice were challenged intranasally with IAV strain X31 (10^3 pfu). **(A)** Mice were monitored for weight loss at indicated time-points. (n = 8). Data represent the mean value ± SEM. Comparisons were made using a repeated-measures two-way ANOVA (Bonferroni post-test). **(B)** Survival was assessed at indicated time points (n = 15). Comparisons were made using log-rank (Mantel-Cox) test **(C)** IAV titre in lungs was determined by plaque assay at 5 d.p.i. (n = 6). Data for individual animals are shown, bars represent the mean ± SD. Mann-Whitney *U* test was used to determine significance. **(D)** The presence of IAV antigen was assessed by IH at 7 d.p.i. (representative images from n = 6).

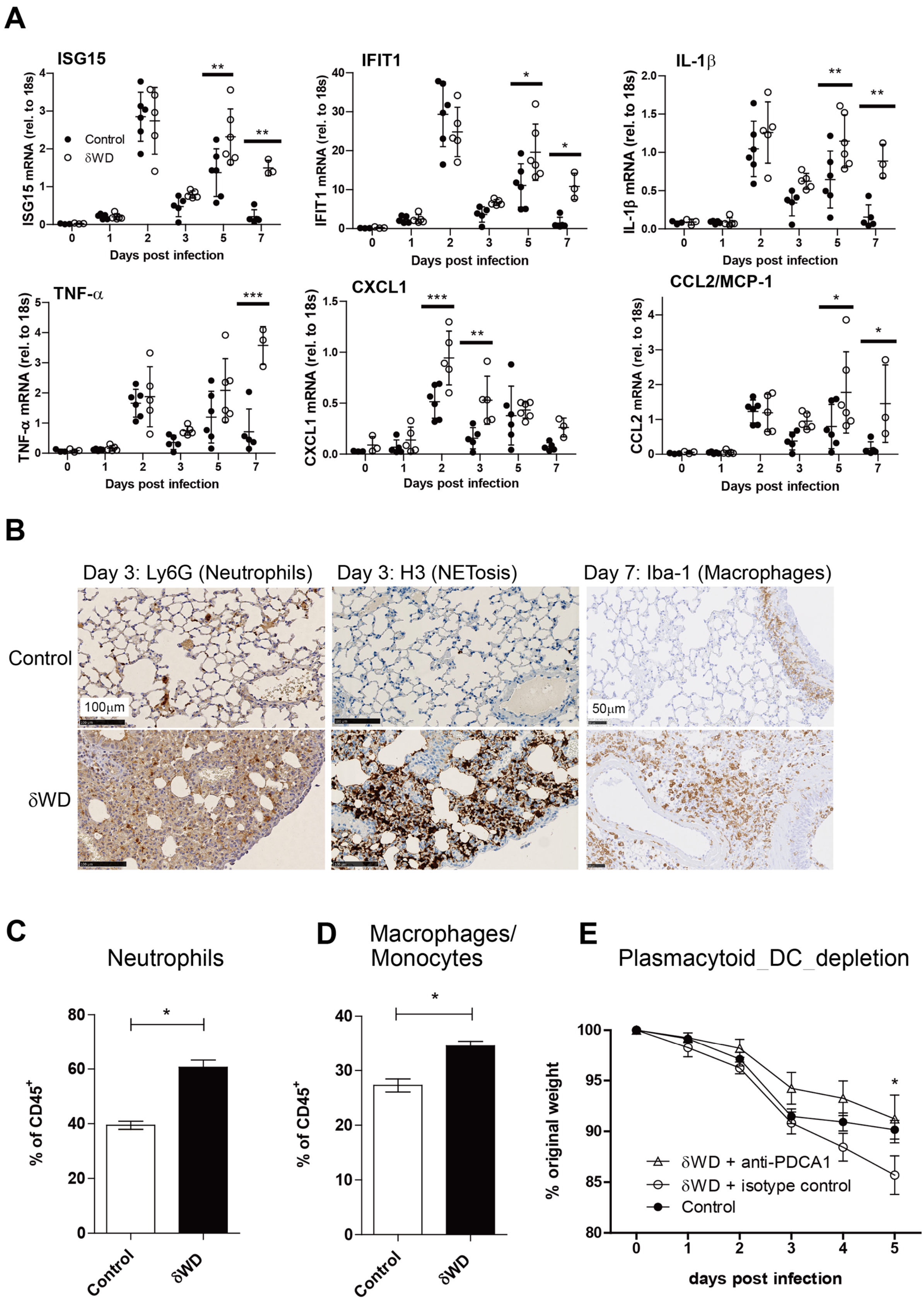
A
ISG15
ISG15 mRNA (rel. to 18s)
Control
δWD
Days post infection
IFIT1
IFIT1 mRNA (rel. to 18s)
IL-1β
IL-1β mRNA (rel. to 18s)
TNF-α
TNF-α mRNA (rel. to 18s)
CXCL1
CXCL1 mRNA (rel. to 18s)
CCL2/MCP-1
CCL2 mRNA (rel. to 18s)
0 1 2 3 5 7
B
Day 3: Ly6G (Neutrophils)
Day 3: H3 (NETosis)
Day 7: Iba-1 (Macrophages)
Control
δWD
100µm
50µm
C
Neutrophils
% of CD45+
Control
δWD
D
Macrophages/ Monocytes
% of CD45+
Control
δWD
E
Plasmacytoid_DC_depletion
% original weight
δWD + anti-PDCA1
δWD + isotype control
Control
days post infection

Fig. 3. Systemic loss of non-canonical autophagy leads to extensive lung inflammation and damage. Littermate control and δWD mice (n = 5) were challenged with IAV X31 (10^3 pfu). (**A)** At the indicated time points, cytokine mRNA transcripts in lung tissue (n = 5) were evaluated by qPCR. Data for individual animals are shown, bars represent the mean ± SD and were compared by 2-way ANOVA with Bonferroni post-tests. (**B**) Representative lung sections from animals (n = 6) taken at 3 d.p.i. were stained by IH for neutrophils (Ly6G) or neutrophil extracellular traps (NET; anti-H3). Sections at 7 d.p.i. were stained for macrophages (Iba-1). Further micrographs are shown in Figs. S1 and S2. **(C)**. BAL (n = 5) was taken at 2 d.p.i and evaluated by flow cytometry, with pre-gating on $CD45^+$. The percentage of neutrophils ($CD11b^+$, $Ly6G^+$) cells is shown ±SEM and were compared using Mann-Whitney *U* test. **(D)**. Single cell suspensions were prepared from lungs taken at 5 d.p.i and evaluated by flow cytometry, with pre-gating on $CD45^+$. The percentage of macrophage/monocytes ($CD11b^+$, $F4/80^+$) cells is shown ±SEM and were compared using Mann-Whitney *U* test. **(E)**. δWD mice were treated with either anti-PCDA-1 (to deplete plasmacytoid DC) or an isotype-matched control. Litter-mate control mice were used as comparator. Weight loss was measured at the indicated days p.i. (n = 5). Comparisons were made using a repeated-measures two-way ANOVA (Bonferroni post-test)

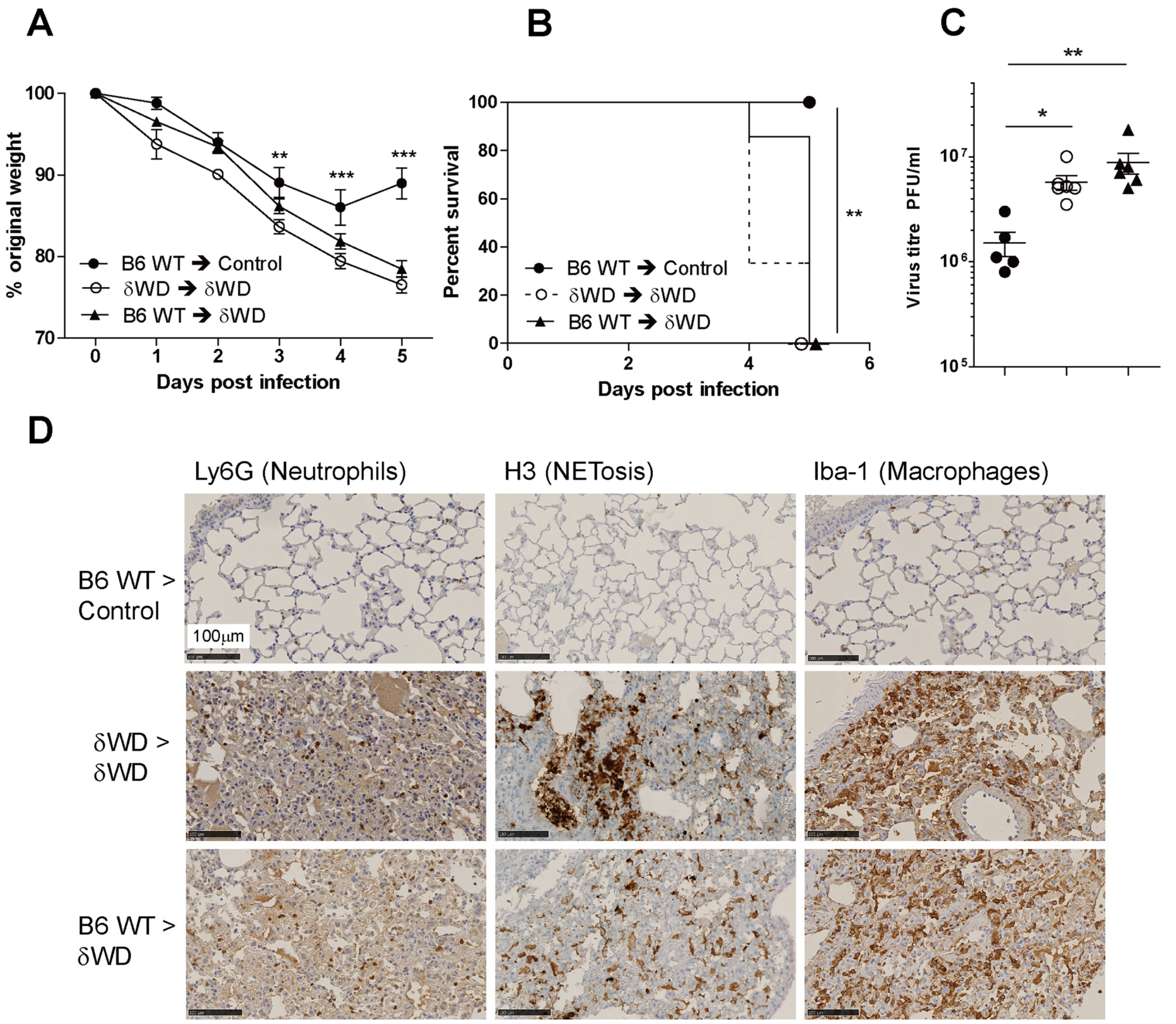

Fig. 4. Bone marrow-derived lymphoid tissue cannot reverse sensitivity to IAV infection Bone marrow from wild-type (*Atg16*L1$^{+/+}$) was used to reconstitute irradiated littermate control mice (B6 WT → control [●]) or δWD mice (B6 WT → δWD [○]). Bone marrow from δWD mice was used to reconstitute irradiated δWD mice (δWD → δWD [▲]). After 12 weeks, mice (n = 5 per group) were challenged with IAV X31 (10^3 pfu). **(A)** Mice were monitored for weight loss at indicated time-points. Data represent the mean value ± SEM. Comparisons were made using a repeated-measures two-way ANOVA (Bonferroni post-test). **(B)** Survival was assessed at indicated time points. Comparisons were made using log-rank (Mantel-Cox) test **(C)** IAV titre in lungs was determined by plaque assay at 5 d.p.i. (n = 6). Data for individual animals are shown,

bars represent the mean ± SD. A one-way ANOVA with Tukey's post-hoc analysis was used to determine significance. **(D)** Lungs taken at 5 d.p.i. were analysed for neutrophils (Ly6G), neutrophil extracellular traps (NET; anti-H3) and macrophages (Iba-1)

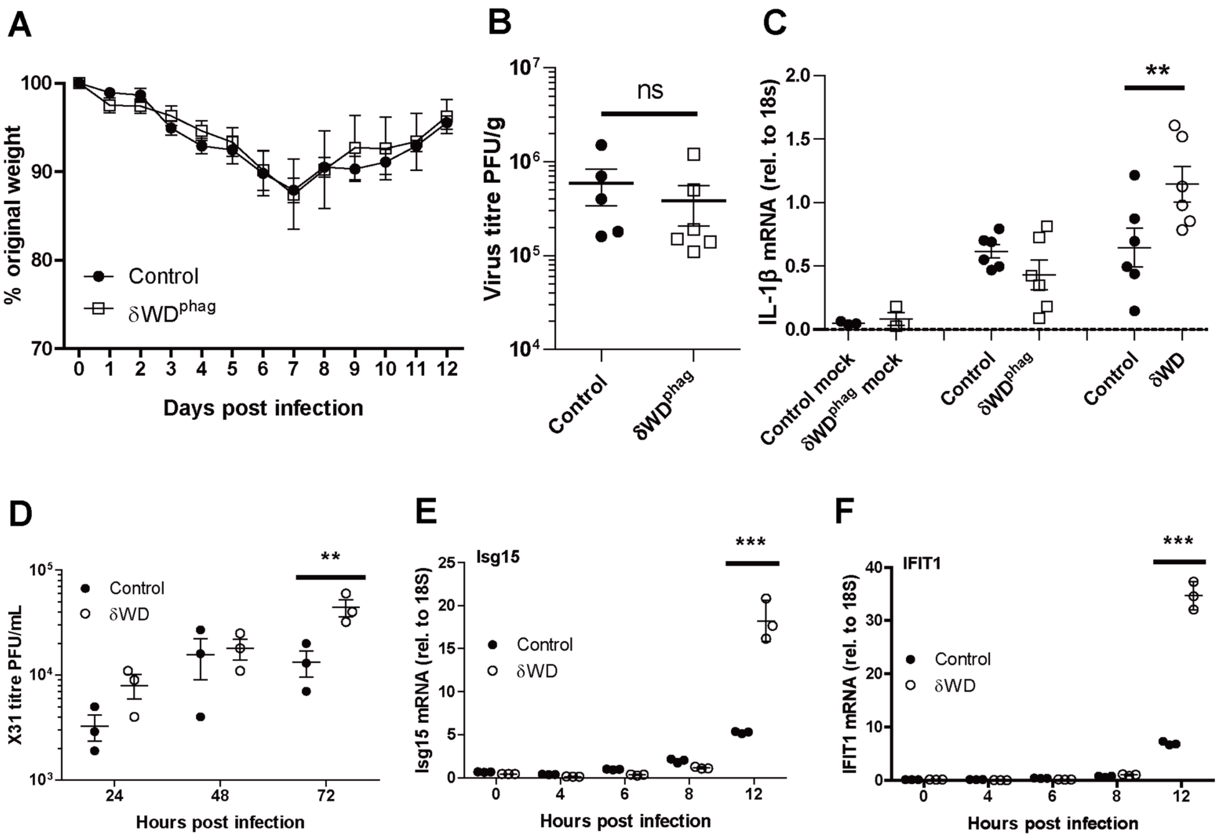

Fig. 5. Non canonical autophagy suppresses IAV replication independently of LAP in phagocytes *in vivo* and *in vitro*. Panels **A to C** δWD^{phag} mice lack non-canonical autophagy in myeloid (LysMcre) cells (for construction see Fig. S6A). Offspring negative for LysMcre were used as littermate controls. Mice (n = 6 per group) were challenged intranasally with IAV X31 (10^3 pfu). **(A)** Mice were monitored for weight loss at indicated time-points. Data represent the mean value ± SEM. Comparisons were made using a repeated-measures two-way ANOVA (Bonferroni post-test). **(B)** IAV titre in lungs was determined by plaque assay at 5 d.p.i. (n = 6). Data for individual animals are shown, bars represent the mean ± SD. Mann-Whitney *U* test was used to determine significance. **(C)** IL-1β mRNA transcripts in lung at 5 d.p.i. were determined by qPCR. Mann-Whitney *U* test was used to determine significance. **(D)** Precision-cut lung slices from control and δWD mice were infected with IAV. Virus titres were determined at indicated time

points. Comparisons were made using two-way ANOVA with Bonferroni post-test. (**E** and **F**) MEFs from δWD or littermate control mice were infected with IAV. At the indicated time points, mRNA transcripts were evaluated by qPCR for **(E)** ISG15 and **(F)** IFIT1. Data for individual animals are shown, bars represent the mean ± SD and were compared by 2-way ANOVA with Bonferroni post-tests.

Materials and Methods

Cell culture and virus.

Influenza virus A/HKx31 (X31, H3N2) was propagated in the allantoic cavity of 9-day-old embryonated chicken eggs at 35˚C for 72 h. Titres were determined by plaque assay using MDCK cells with an Avicel overlay.

Mice.

All experiments were performed in accordance with UK Home Office guidelines and under the UK Animals (Scientific procedures) Act1986.

The generation of δWD mice (*Atg16L1*$^{\delta WD/\delta WD}$) has been described previously [21]. Generation of δWD^{phag} and *Atg16L1*$^{fl/fl}$-LysMCre mice is described in detail in Fig. S7. Comparisons were made using age and sex-matched littermate control mice for each individual genotype. Generation and breeding of mice was approved by the University of East Anglia Animal Welfare and Ethical Review Body and performed under UK Home Office Project License 70/8232.

Influenza Infection studies were performed at the University of Liverpool, approved by the University of Liverpool Animal Welfare and Ethical Review Body and performed under UK Home Office Project License 70/8599. Studies used 2-3 m old male and female mice that had been back-crossed to C57BL/6J. Mice were maintained under specific pathogen-free barrier conditions in individually ventilated cages (Greenline GM500, Techniplast) at a temperature of 22°C (± 2°C), humidity 55% (± 10%), light/dark cycle 12/12 hours (7 am to 7 pm), food CRM(P) and RO or filtered water *ad lib*. Colonies were screened using the Charles River surveillance plus PRIA health screening profile every 3 months to ensure SPF status.

For IAV infection, animals were randomly assigned into multiple cohorts, anaesthetised lightly by the i.m. route with 150 mg/kg ketamine (Ketavet, Zoetis UK Ltd) and separate cohorts inoculated intra-nasally with 10^3 PFU IAV strain X31 in 50 µl sterile PBS. Mice were infected between 9 and 11 AM. Animals were sacrificed at variable time-points after infection by cervical dislocation. Tissues were removed immediately for downstream processing. Sample sizes of n = 6 were used as determined using power calculations and previous experience of experimental infection with these viruses. For survival analysis, a humane endpoint was determined using a scoring matrix that included excessive (>20%) weight loss.

To specifically deplete plasmacytoid dendritic cells (pDCs), mice were treated with anti-PDCA-1 (Cambridge Bioscience) or IgG2b isotype-matched control, using a dose of 500 mg per 200 ml via the i.p. route on day 1 of infection with IAV and every 48 h thereafter [27].

Generation and analysis of radiation chimeras

The general strategy is shown in Fig S6A. Mice were subjected to whole body irradiation with 11 Gy in two doses 4 h apart using a ^{137}Cs source in a rotating closed chamber. Bone marrow was collected from male wild-type C57BL/6-Ly5.1 (B6.SJL-*Ptprc*^{a}*Pepc*^{b}/BoyCrl; Atg16L1$^{+/+}$) mice that are congenic for the CD45.1 allele or from δWD mice (that are congenic for CD45.2). The C57BL/6 CD45.1 marrows were used to enable confirmation of chimaerism by FACS analysis of bon-marrow-derived cells as littermate control and δWD mice are CD45.2 (Fig S6B). The femur and tibia of the donor mouse was collected and sterilised for 2 min in 70% ethanol. The ends of the bones were removed and PBS was used to flush out the bone marrow through a 40 μm cell sieve. Red blood cell lysis was performed using 0.83% ammonium chloride and the cells were washed twice in PBS and re-suspended at a concentration of 10^7 cells/ml. T cell depletion was performed prior to transfusion by using a commercial mouse hematopoietic progenitor cell isolation kit (EasySep, STEMCELL™ Technologies, #19856).

After depletion, 10^6 donor bone marrow cells were injected into each irradiated mouse by tail vein injection 3 h following irradiation. Mice were then allowed to recover for 12 weeks with daily monitoring of mouse weights and general condition for at least the first two weeks to monitor for any severe radiation sickness or illness due to being immunocompromised.

For chimaerism analysis, approximately10^6 spleen cells were analysed by flow cytometry using fluorochrome-conjugated monoclonal antibodies specific for CD45.1 (clone A20 eBioscience), CD45.2, (clone 104 eBioscience). As shown in Fig. S6B, in the groups where CD45.1 marrow was transplanted all mice were >95% chimaeric.

Flow Cytometric analysis of Cells.

Brocho-alvolear lavage fluid (BAL) was obtained by lavage of mice via the trachea using 1 ml ice-cold RPMI containing 5% FCS. For lung tissue, single-cell suspensions were made from minced lung and subjected to collagenase and DNase I digestion, then treated with ACK buffer to remove red blood cells. In both cases, approximately10^6 cells were incubated in 100 μl of Fc block (clone 2.4G2, BD Bioscience) diluted in PBS, 2% FCS (PBS-FCS) for 15 min at 4 °C prior to the addition of fluorochrome-conjugated monoclonal antibodies and incubation for 30 min at 4°C in the dark. Cells were then washed in PBS-

FCS, fixed in 4% paraformaldehyde in PBS for 15 min at 20°C prior to analysis on a MACSQuant Analyzer 10 (Miltenyi Biotech UK). Data were analysed using FlowJo (FlowJo, LLC). Antibodies used included: CD45, Ly6G, CD11c, CD11b, F4/80 (all eBioscience). Neutrophil populations in BAL were identified as $CD45^+$, $CD11c^-$, $CD11b^+$, $Ly6G^+$. Macrophage/monocyte populations in lung tissue were identified as $CD45^+$, $CD11c^-$, $CD11b^+$, $F4/80^+$.

Histology, immunohistochemistry. Tissues were fixed in 4% buffered paraformaldehyde (PFA; pH7.4) for 24 h and routinely paraffin wax embedded. Consecutive sections (3-5 µm) were either stained with haematoxylin and eosin (HE) or used for immunohistochemistry (IH).

IH was performed to detect influenza antigens and to identify neutrophils and neutrophil extracellular traps (NETs) and macrophages using the horseradish peroxidase (HRP) and the avidin biotin complex (ABC) method. The following primary antibodies were applied: goat anti-IAV (Meridian Life Sciences Inc., B65141G), rat anti-mouse Ly6G (clone 1A8, Biolegend; neutrophil marker), rabbit anti-Iba-1 (antigen: AIF1; Wako Chemicals; microglia/macrophage specific marker), and rabbit anti-histone H3 (citrulline R2 + R8 + R17; Abcam; NET marker). Briefly, after deparaffination, sections underwent antigen retrieval in citrate buffer (pH 6.0, 20 min at 98°C) followed by blocking of endogenous peroxidase (peroxidase block, S2023, Dako) for 10 min at room temperature (RT). Slides were then incubated with the primary antibodies (diluted in dilution buffer, Dako) for a) Iba-1 (60 min at RT), followed by a 30 min incubation at room temperature with the secondary antibody (Envision mouse and rabbit, respectively, Dako) in an autostainer (Dako), and b) Ly6G (60 min at RT), followed by rabbit anti-rat IgG and the ABC kit (both 30 min at RT; Ventana). Staining for histone H3 was undertaken with an autostainer (Discovery XT, Ventana), using citrate buffer, dilution buffer and detection kits provided by the manufacturer. The antibody reaction was visualized with 3,3'-diaminobenzidine and sections counterstained with haematoxylin.

Statistical analysis. Data were analysed using the Prism package (version 5.04 Graphpad Software). *P* values were set at 95% confidence interval. A repeated-measures two-way ANOVA (Bonferroni post-test) was used for time-courses of weight loss; two-way ANOVA (Bonferroni post-test) was used for other time-courses; log-rank (Mantel-Cox) test was used for survival curves; one-way ANOVA (Tukey's post-hoc) was used to compare three or more groups side-by-side; Mann-Whitney *U* test was used to compare two groups. All differences not specifically stated to be significant were not significant ($p > 0.05$). For all figures, *p < 0.05, **p <0.01, ***p < 0.001, ****p < 0.0001.

Cells and cell culture. Mouse embryonic fibroblasts (MEFs) were generated by serial passage of cells taken from mice at embryonic day 13.5 and cultured in DMEM (ThermoFisher scientific, 11570586) with 10% FCS. Bone marrow derived macrophages (BMDMs) were generated from femur and tibia flushed with RPMI-1640 (Sigma, R8758). Macrophages were generated from adherent cells in RPMI-1640 containing 10% FCS and M-CSF (Peprotech, 315-02) (30 ng/ml) for 6 d. Macrophage populations were quantified by FACS using antibodies against CD16/CD32, F4/80 and CD11b (BioLegend, 101320, 123107).

Precision-cut lung slices

Infection of *ex vivo* lung slices was used to examine the responses of lungs without any contribution from recruited leukocytes, which could not be present. Mouse lungs were inflated with 2% low melting point agarose in HBSS and then sliced into 300 μm sections using a vibrating microtome. They were then cultured overnight in DMEM/F12 medium (Thermofisher 21331020) prior to infection with IAV.

Autophagy and non-canonical autophagy.

Autophagy was activated by incubating cells in Hanks balanced salt solution (HBSS) (ThermoFisher, 11550456) for 2 h at 37°C. Non-canonical autophagy was stimulated in BMDMs by incubation with Zymosan A (Alexa Fluor 594-labelled; Thermofisher Z23374). LC3 was analyzed by immunofluorescence microscopy and LC3i:LC3II Western blot.

qPCR for cytokine transcription.

Lung lobes were snap frozen and homogenized using a TissueLyser (Qiagen). Tissue culture cells were washed twice using PBS. Total RNA was extracted by Trizol-chloroform (Thermofisher 15596018) and purified by RNeasy MinElute cleanup kit (Qiagen 74204). RNA was analysed by qPCR using SYBR Green/7500 (Thermofisher S7563) standard Real-Time PCR system (Applied Biosystems, Grand Island, NY) and primer sets as detailed in Table S1. Relative amounts of mRNA expression were normalized to 18S rRNA.

Table 1. Primer sequences for mRNAs analysed by RT-qPCR.

Target	**Catalogue number**†
ISG15	QT00322749
IFIT1	QT01161286
IL-1β	QT01048355
TNF-α	QT00104006
CXCL1	QT00115647
CCL2/MCP-1	QT00167832
18S ribosomal RNA	QT02448075

† Catalogue numbers refer to validated QuantiTect primer sets (Qiagen)

Western blotting. Cells were lysed using M-PER reagent (ThermoFisher 78501) with complete protease inhibitor cocktail (Sigma, 04693159001) and clarified by centrifugation. Extracted proteins (20 μg) were separated on a precast 4–12% gradient SDS-PAGE gels (Expedeon, NBT41212), transferred to immobilon PVDF (Millipore, IPFL00010) and probed using antibodies for ATG16L1 (MBL M150-3), LC3A/B (Cell signaling 41085) and actin (Sigma, A5441). Primary antibodies were detected using IRDye labelled secondary antibodies (LI-COR biosciences, 926-32211, 926-68020) and visualised by Odyssey infrared system (LI-COR).

Fluorescence imaging*.* Cells were fixed in ice cold methanol and non-specific binding was blocked using 5% goat serum plus 0.3% Triton-X100 in PBS followed by incubating with anti LC3A/B (Cell Signalling 4108) or anti-ATG16L1 (MBL M150-3). Cells were washed and then incubated with anti-rabbit-Alexa 488 (Thermofisher 10729174). After washing, cells were counterstained with 4’, 6 diamidino-2-phenylindole (DAPI) (ThermoFisher scientific, 10116287) and mounted with Fluoromount-G (Cambridge Bioscience). Cells were imaged on a Zeiss Imager M2 Apotome microscope with a 63x, 1.4 NA oil-immersion objective.

REFERENCES

1 Delgado, M. A., Elmaoued, R. A., Davis, A. S., Kyei, G. & Deretic, V. Toll-like receptors control autophagy. *EMBO J.* **27**, 1110-1121, doi:10.1038/emboj.2008.31 (2008).

2 Fletcher, K. *et al.* The WD40 domain of ATG16L1 is required for its non-canonical role in lipidation of LC3 at single membranes. *EMBO J.* **37**, doi:10.15252/embj.201797840 (2018).

3 Lamprinaki, D. *et al.* LC3-Associated Phagocytosis Is Required for Dendritic Cell Inflammatory Cytokine Response to Gut Commensal Yeast Saccharomyces cerevisiae. *Front Immunol* **8**, 1397, doi:10.3389/fimmu.2017.01397 (2017).

4 Martinez, J. *et al.* Molecular characterization of LC3-associated phagocytosis reveals distinct roles for Rubicon, NOX2 and autophagy proteins. *Nat Cell Biol* **17**, 893-906, doi:10.1038/ncb3192 (2015).

5 Sanjuan, M. A. *et al.* Toll-like receptor signalling in macrophages links the autophagy pathway to phagocytosis. *Nature* **450**, 1253-1257, doi:10.1038/nature06421 (2007).

6 Heckmann, B. L. *et al.* LC3-Associated Endocytosis Facilitates beta-Amyloid Clearance and Mitigates Neurodegeneration in Murine Alzheimer's Disease. *Cell* **178**, 536-551 e514, doi:10.1016/j.cell.2019.05.056 (2019).

7 Tan, J. M. J. *et al.* An ATG16L1-dependent pathway promotes plasma membrane repair and limits Listeria monocytogenes cell-to-cell spread. *Nat Microbiol* **3**, 1472-1485, doi:10.1038/s41564-018-0293-5 (2018).

8 Florey, O., Gammoh, N., Kim, S. E., Jiang, X. & Overholtzer, M. V-ATPase and osmotic imbalances activate endolysosomal LC3 lipidation. *Autophagy* **11**, 88-99, doi:10.4161/15548627.2014.984277 (2015).

9 Florey, O., Kim, S. E., Sandoval, C. P., Haynes, C. M. & Overholtzer, M. Autophagy machinery mediates macroendocytic processing and entotic cell death by targeting single membranes. *Nat Cell Biol* **13**, 1335-1343, doi:10.1038/ncb2363 (2011).

10 Roberts, R. *et al.* Autophagy and formation of tubulovesicular autophagosomes provide a barrier against nonviral gene delivery. *Autophagy* **9**, 667-682, doi:10.4161/auto.23877 (2013).

11 Gluschko, A. *et al.* The beta2 Integrin Mac-1 Induces Protective LC3-Associated Phagocytosis of Listeria monocytogenes. *Cell Host Microbe* **23**, 324-337 e325, doi:10.1016/j.chom.2018.01.018 (2018).

12 Hubber, A. *et al.* Bacterial secretion system skews the fate of Legionella-containing vacuoles towards LC3-associated phagocytosis. *Sci Rep* **7**, 44795, doi:10.1038/srep44795 (2017).

13 Matte, C. *et al.* Leishmania major Promastigotes Evade LC3-Associated Phagocytosis through the Action of GP63. *PLoS Pathog* **12**, e1005690, doi:10.1371/journal.ppat.1005690 (2016).

14 Akoumianaki, T. *et al.* Aspergillus Cell Wall Melanin Blocks LC3-Associated Phagocytosis to Promote Pathogenicity. *Cell Host Microbe* **19**, 79-90, doi:10.1016/j.chom.2015.12.002 (2016).

15 Kyrmizi, I. *et al.* Calcium sequestration by fungal melanin inhibits calcium-calmodulin signalling to prevent LC3-associated phagocytosis. *Nat Microbiol* **3**, 791-803, doi:10.1038/s41564-018-0167-x (2018).

16 Lu, Q. *et al.* Homeostatic Control of Innate Lung Inflammation by Vici Syndrome Gene Epg5 and Additional Autophagy Genes Promotes Influenza Pathogenesis. *Cell Host Microbe* **19**, 102-113, doi:10.1016/j.chom.2015.12.011 (2016).

17 Saitoh, T. *et al.* Loss of the autophagy protein Atg16L1 enhances endotoxin-induced IL-1beta production. *Nature* **456**, 264-268, doi:10.1038/nature07383 (2008).

18 Yang, C. S. *et al.* NADPH oxidase 2 interaction with TLR2 is required for efficient innate immune responses to mycobacteria via cathelicidin expression. *J. Immunol.* **182**, 3696-3705, doi:10.4049/jimmunol.0802217 (2009).

19 Yang, C. S. *et al.* The autophagy regulator Rubicon is a feedback inhibitor of CARD9-mediated host innate immunity. *Cell Host Microbe* **11**, 277-289, doi:10.1016/j.chom.2012.01.019 (2012).

20 Martinez, J. *et al.* Noncanonical autophagy inhibits the autoinflammatory, lupus-like response to dying cells. *Nature* **533**, 115-119, doi:10.1038/nature17950 (2016).

21 Rai, S. *et al.* The ATG5-binding and coiled coil domains of ATG16L1 maintain autophagy and tissue homeostasis in mice independently of the WD domain required for LC3-associated phagocytosis. *Autophagy* **15**, 599-612, doi:10.1080/15548627.2018.1534507 (2019).

22 Lystad, A. H. *et al.* Distinct functions of ATG16L1 isoforms in membrane binding and LC3B lipidation in autophagy-related processes. *Nat Cell Biol* **21**, 372-383, doi:10.1038/s41556-019-0274-9 (2019).

23 Dooley, H. C. *et al.* WIPI2 links LC3 conjugation with PI3P, autophagosome formation, and pathogen clearance by recruiting Atg12-5-16L1. *Mol. Cell* **55**, 238-252, doi:10.1016/j.molcel.2014.05.021 (2014).

24 Yamayoshi, S. & Kawaoka, Y. Current and future influenza vaccines. *Nat. Med.* **25**, 212-220, doi:10.1038/s41591-018-0340-z (2019).

25 Teijaro, J. R., Walsh, K. B., Rice, S., Rosen, H. & Oldstone, M. B. Mapping the innate signaling cascade essential for cytokine storm during influenza virus infection. *Proc. Natl. Acad. Sci. U. S. A.* **111**, 3799-3804, doi:10.1073/pnas.1400593111 (2014).

26 Ramos, I. & Fernandez-Sesma, A. Modulating the Innate Immune Response to Influenza A Virus: Potential Therapeutic Use of Anti-Inflammatory Drugs. *Front Immunol* **6**, 361, doi:10.3389/fimmu.2015.00361 (2015).

27 Davidson, S., Crotta, S., McCabe, T. M. & Wack, A. Pathogenic potential of interferon alphabeta in acute influenza infection. *Nat Commun* **5**, 3864, doi:10.1038/ncomms4864 (2014).

28 Iwasaki, A. & Pillai, P. S. Innate immunity to influenza virus infection. *Nat Rev Immunol* **14**, 315-328, doi:10.1038/nri3665 (2014).

29 Herold, S., Becker, C., Ridge, K. M. & Budinger, G. R. Influenza virus-induced lung injury: pathogenesis and implications for treatment. *Eur. Respir. J.* **45**, 1463-1478, doi:10.1183/09031936.00186214 (2015).

30 Skehel, J. J. & Wiley, D. C. Receptor binding and membrane fusion in virus entry: the influenza hemagglutinin. *Annu. Rev. Biochem.* **69**, 531-569, doi:10.1146/annurev.biochem.69.1.531 (2000).

31 Wharton, S. A., Belshe, R. B., Skehel, J. J. & Hay, A. J. Role of virion M2 protein in influenza virus uncoating: specific reduction in the rate of membrane fusion between virus and liposomes by amantadine. *J. Gen. Virol.* **75 (Pt 4)**, 945-948, doi:10.1099/0022-1317-75-4-945 (1994).

32 Boulo, S., Akarsu, H., Ruigrok, R. W. & Baudin, F. Nuclear traffic of influenza virus proteins and ribonucleoprotein complexes. *Virus Res.* **124**, 12-21, doi:10.1016/j.virusres.2006.09.013 (2007).

33 Belser, J. A. *et al.* Pathogenesis and transmission of triple-reassortant swine H1N1 influenza viruses isolated before the 2009 H1N1 pandemic. *J. Virol.* **85**, 1563-1572, doi:10.1128/JVI.02231-10 (2011).

34 Szretter, K. J. *et al.* Role of host cytokine responses in the pathogenesis of avian H5N1 influenza viruses in mice. *J. Virol.* **81**, 2736-2744, doi:10.1128/JVI.02336-06 (2007).

35 Akram, K. M. *et al.* An innate defense peptide BPIFA1/SPLUNC1 restricts influenza A virus infection. *Mucosal Immunol* **11**, 71-81, doi:10.1038/mi.2017.45 (2018).

36 Boada-Romero, E. *et al.* The T300A Crohn's disease risk polymorphism impairs function of the WD40 domain of ATG16L1. *Nat Commun* **7**, 11821, doi:10.1038/ncomms11821 (2016).

37 Kreibich, S. *et al.* Autophagy Proteins Promote Repair of Endosomal Membranes Damaged by the Salmonella Type Three Secretion System 1. *Cell Host Microbe* **18**, 527-537, doi:10.1016/j.chom.2015.10.015 (2015).

38 Huang, J. *et al.* Activation of antibacterial autophagy by NADPH oxidases. *Proc. Natl. Acad. Sci. U. S. A.* **106**, 6226-6231, doi:10.1073/pnas.0811045106 (2009).

39 Wei, H., Gan, B., Wu, X. & Guan, J. L. Inactivation of FIP200 leads to inflammatory skin disorder, but not tumorigenesis, in conditional knock-out mouse models. *J. Biol. Chem.* **284**, 6004-6013, doi:10.1074/jbc.M806375200 (2009).

40 Heckmann, B. L., Boada-Romero, E., Cunha, L. D., Magne, J. & Green, D. R. LC3-Associated Phagocytosis and Inflammation. *J. Mol. Biol.* **429**, 3561-3576, doi:10.1016/j.jmb.2017.08.012 (2017).

41 Ullrich, S. *et al.* The novel membrane protein TMEM59 modulates complex glycosylation, cell surface expression, and secretion of the amyloid precursor protein. *J. Biol. Chem.* **285**, 20664-20674, doi:10.1074/jbc.M109.055608 (2010).

42 Berryman, S. *et al.* Foot-and-mouth disease virus induces autophagosomes during cell entry via a class III phosphatidylinositol 3-kinase-independent pathway. *J. Virol.* **86**, 12940-12953, doi:10.1128/JVI.00846-12 (2012).

43 Kemball, C. C. *et al.* Coxsackievirus infection induces autophagy-like vesicles and megaphagosomes in pancreatic acinar cells in vivo. *J. Virol.* **84**, 12110-12124, doi:10.1128/JVI.01417-10 (2010).

Supplementary Materials for:

The WD and linker domains of ATG16L1 required for non-canonical autophagy limit lethal influenza A virus infection at epithelial surfaces.

Yingxue Wang, Weijiao Zhang, Matthew Jefferson, Parul Sharma, Ben Bone, Anja Kipar, Janine L. Coombes, Timothy Pearson, Angela Man, Alex Zhekova, Yongping Bao, Ralph A Tripp, Simon R. Carding, Ulrike Mayer, Penny P. Powell, James P. Stewart & Thomas Wileman

Correspondence to: t.wileman@uea.ac.uk and j.p.stewart@liv.ac.uk

This PDF file includes:

Figs. S1 to S8

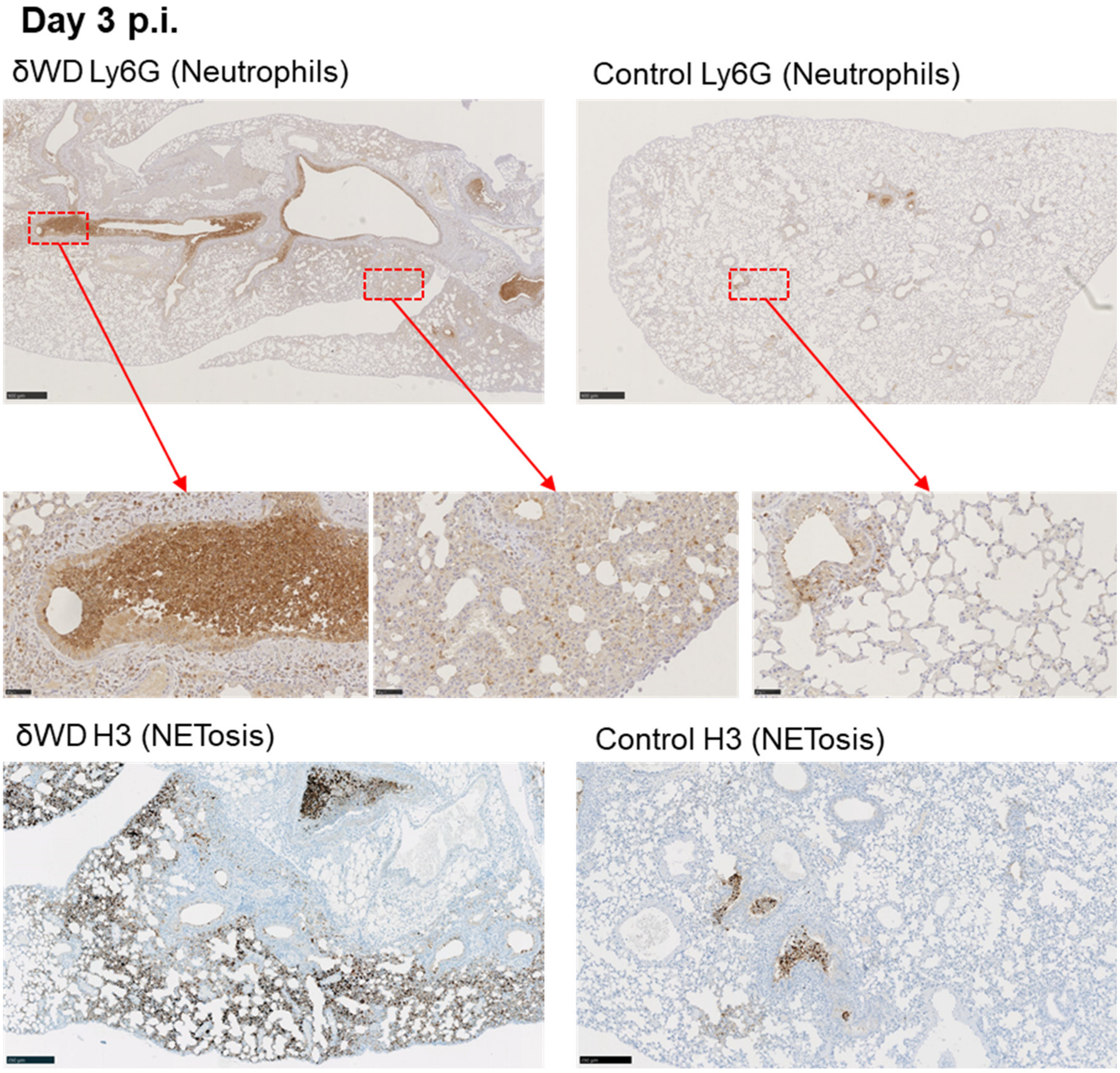

Fig. S1. Increased neutrophilia and NETosis in IAV-infected mice deficient in non-canonical autophagy

δWD and littermate control mice were infected i.n. with 10^3 pfu IAV X31. Lung tissues were harvested at 3d p.i. Neutrophils and H3 (marker of NETosis) were detected by IH using anti-Ly6G and anti-H3, visualized with DAB and counter-stained with hematoxylin. Micrographs of representative areas from lungs of six mice are shown. Scale bars represent 500 μm (upper panels), 50 μm (middle panels) or 250 μm (lower panels). There are dramatically increased numbers of neutrophils in airways (bronchi and bronchioles) and lung parenchyma of δWD mice, accompanied by markedly-increased NETosis, indicating significant neutrophil degeneration.

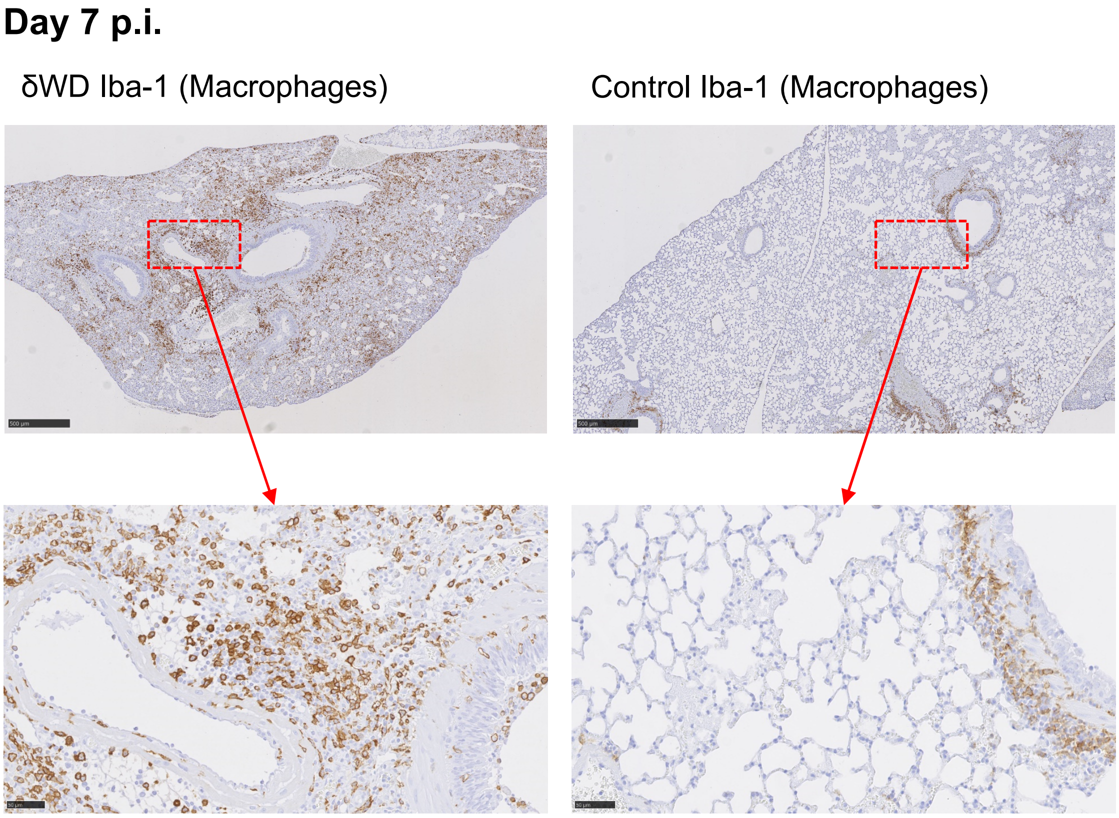
Day 7 p.i.

δWD Iba-1 (Macrophages)

Control Iba-1 (Macrophages)

Fig. S2. Increased macrophage rich inflammation in IAV-infected mice deficient in non-canonical autophagy

δWD and littermate control mice were infected i.n. with 10^3 pfu IAV X31. Lung tissues were harvested at 7d p.i. Macrophages were detected by IH using anti-Iba-1, visualized with DAB and counter-stained with hematoxylin. Micrographs of representative areas from lungs of six mice are shown. Scale bars represent 500 µm (upper panels) and 50 µm (lower panels). Lower panels are the same as in Fig. 2B. Upper panels show the lower magnification images of the lung to illustrate the general nature of the observations. There is clearly increased inflammation in δWD mice with higher numbers of macrophages in the lung parenchyma.

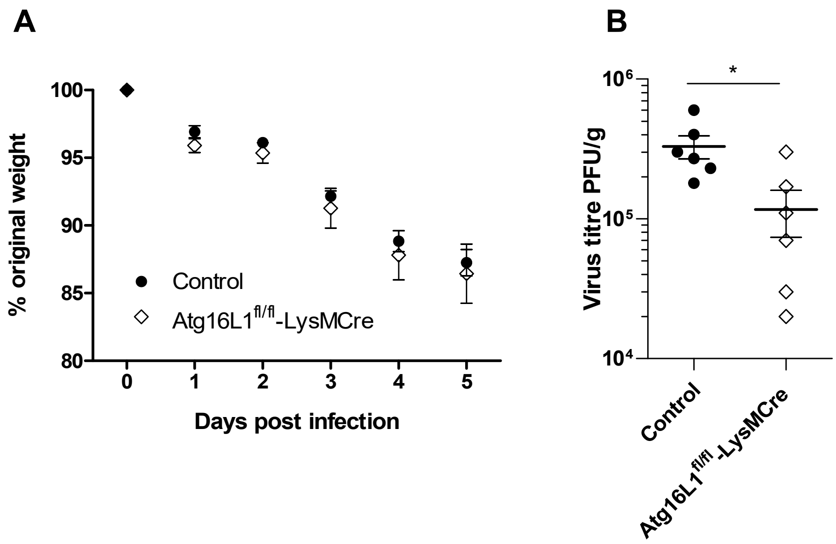

Fig. S3. **LysMcre-mediated loss of canonical macro-autophagy from phagocytes decreases sensitivity to IAV infection**

*Atg*16L1$^{fl/fl}$-LysMcre mice and littermate controls; *n* = 5 or 6 per group) were infected i.n. with 10^3 pfu IAV X31. **Panel A.** Mice were weighed daily and the weights presented as a percentage of the starting weight. **Panel B.** Lung tissues were taken at 5 d.p.i. and virus titer determined by plaque assay. Data represent the mean value ± SEM. Analysis using the Mann-Whitney U test showed a significant difference (* $p < 0.05$). Thus, *Atg*16L1$^{fl/fl}$-LysMcre mice that are deficient in canonical autophagy in phagocytes lose weight at the same rate as littermate controls but are more resistant to virus replication as they have lower lung virus titres.

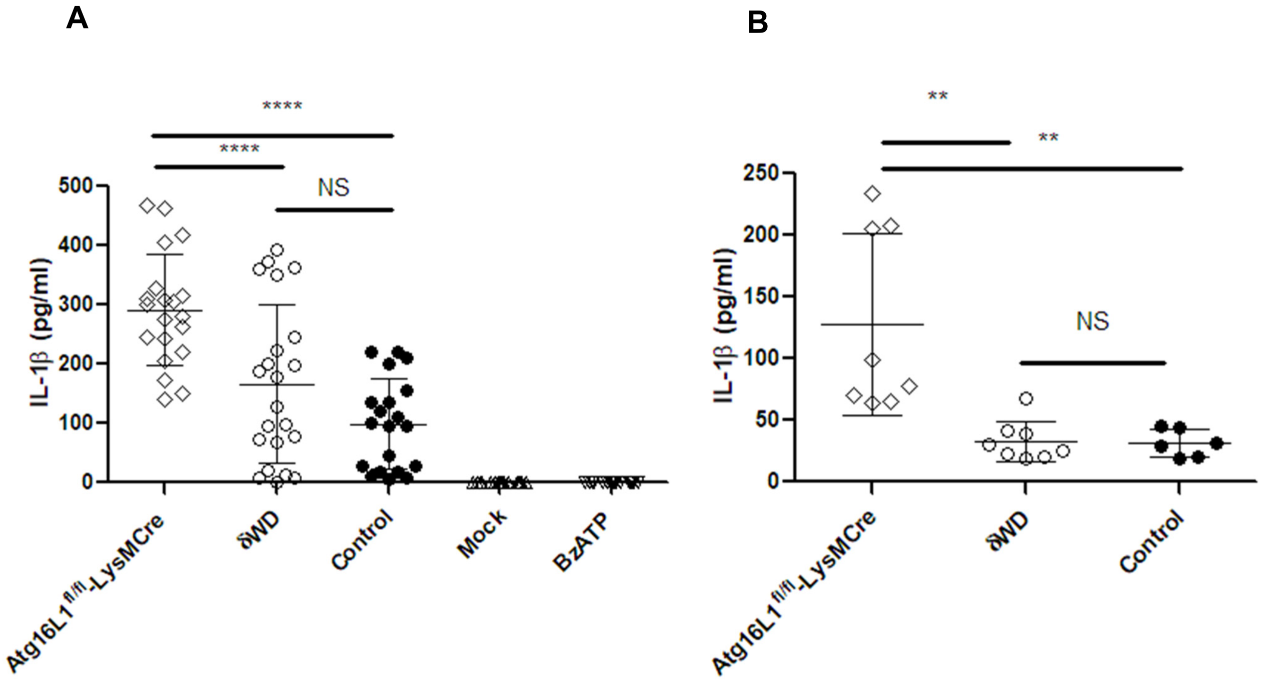

Fig. S4. Mice deficient in non-canonical autophagy do not have elevated IL-1β in response to LPS stimulation

LysMcre-mediated deletion of autophagy genes from mice leads to increased inflammatory threshold characterised by raised secretion of IL-1β from macrophages (*15*), and in the lung this can increase resistance to IAV infection (*16*). The possibility that the δWD mutation could affect IL-1β secretion was tested by stimulating BMDM with bacterial lipopolysaccharide (LPS) and BzATP ($P2X_7$ receptor agonist) or challenging mice with LPS.

Panel A. Bone marrow-derived macrophages (BMDM) from mice strains as indicated were incubated with 100 ng/ml of LPS for 4 h and 150 μM of BzATP for 30 min. Supernatants were assayed for IL-1β by ELISA. (Mock group: untreated, BzATP controls only received BzATP). Representative data are shown as the means ± SD of readings from 20 wells per group and were analyzed using one-way ANOVA with Tukey's post-hoc analysis (**** *p*<0.0001). Approximately three-fold increases in IL-1β secretion were seen for BMDM from Atg16L1$^{fl/fl}$-LysMCre mice. However, IL-1β secretion from δWD BMDM did not differ significantly from littermate controls.

Panel B. Mouse strains (as indicated) were injected with 20 mg/kg of LPS via the IP route. Serum collected 90 min post injection was assayed for IL-1β by ELISA. In non-treated mice IL-1β was below the detection limit in all 3 strains (not shown). Data are shown as the means ± SD of duplicate assays from 4 mice per group and were analyzed using one-way ANOVA with Tukey's post-hoc analysis (** *p* < 0.01). Approximately three-fold increases in IL-1β secretion were seen for *Atg*16L1$^{fl/fl}$-LysMCre, however IL-1β secretion for δWD mice did not differ significantly from littermate controls.

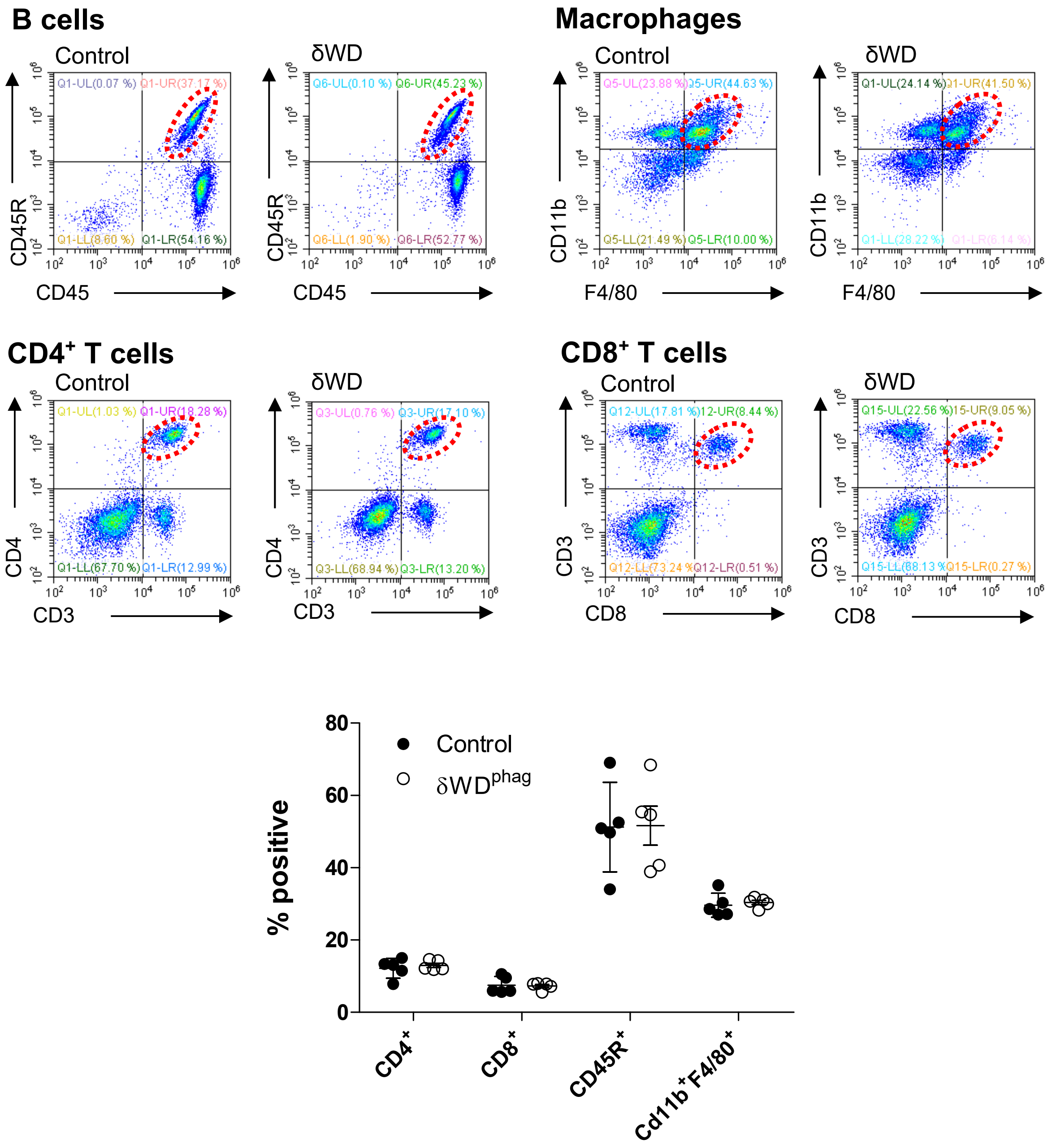

Fig. S5. Mice deficient in non-canonical autophagy have normal leukocyte populations

The possibility that the loss of non-canonical autophagy resulted in changes in leukocyte populations was tested by analysing dissociated spleens by FACS using antibodies to T-cell subsets (CD3$^+$, CD4$^+$ and CD3$^+$, CD8$^+$), B-cells (CD45R/B220) and macrophages (CD11b, F40/80) Upper panel shows representative FACS profiles from n = 3 mice. Lower panel shows the percentage positive for each population.

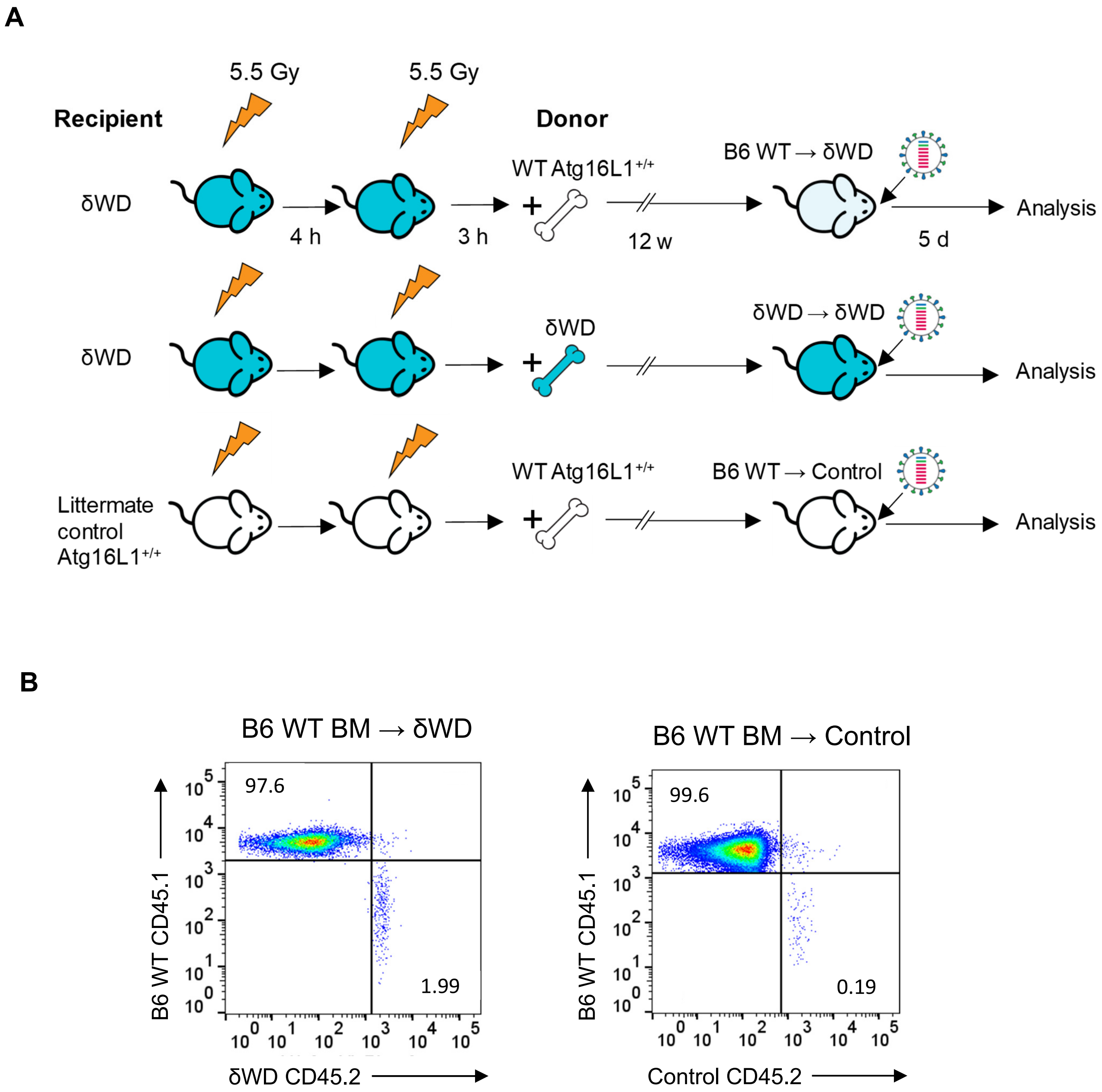

Fig. S6. Confirmation of bone marrow transplant radiation chimaerism

Panel A. Strategy for making bone-marrow chimaeras. **Panel B**. Chimaerism was confirmed 12 weeks post-transplant in spleen cells by flow-cytometric analysis of congenic markers on leukocytes (CD45.1, CD45.2). Flow plot shows representative plot from one C57BL/6 WT (CD45.1) bone-marrow → δWD (CD45.2) recipient chimaera and one C57BL/6 WT (CD45.1) bone-marrow → littermate control (CD45.2) recipient chimaera. All animals were > 95% chimaeric.

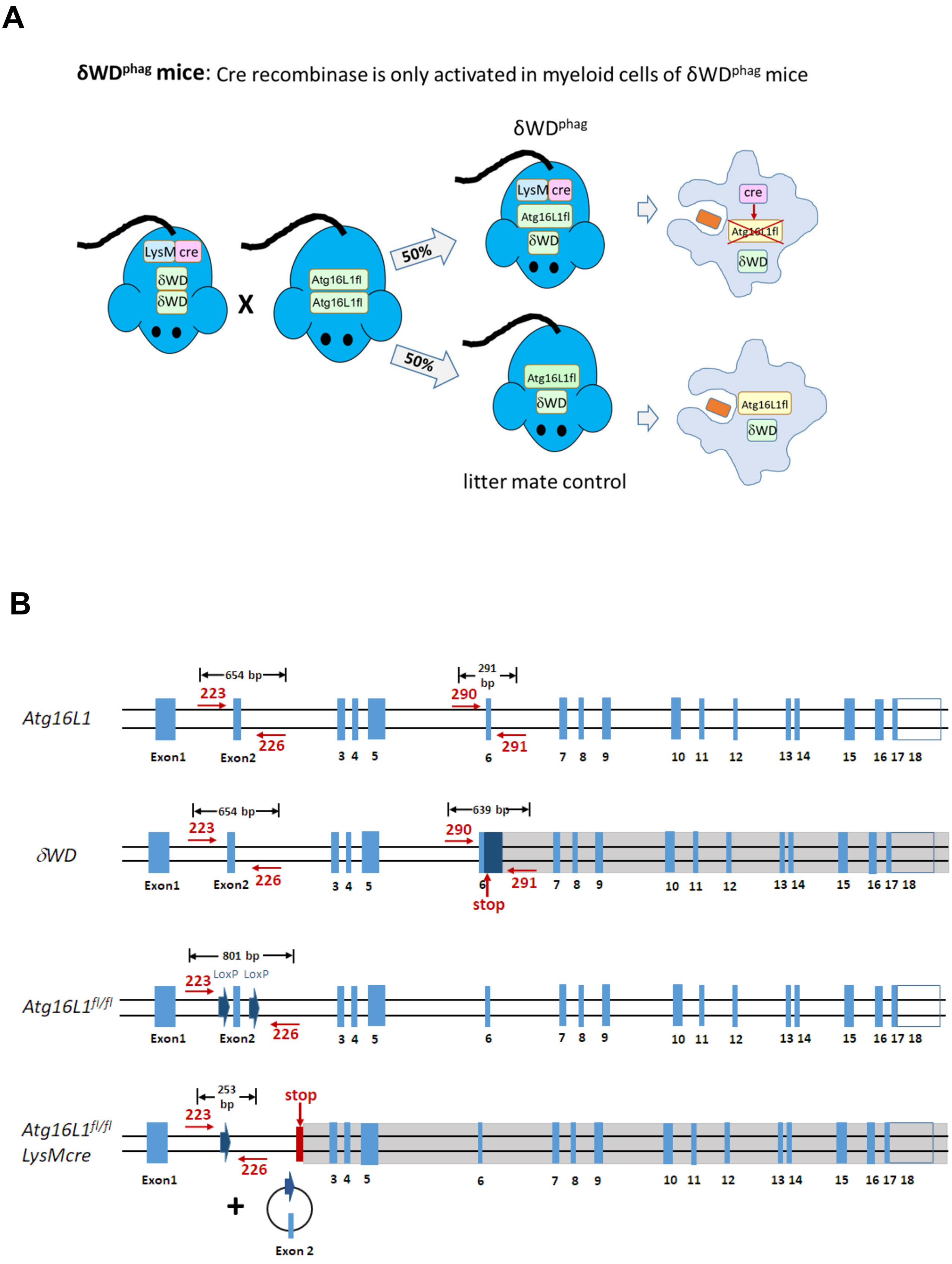
A
δWDphag mice: Cre recombinase is only activated in myeloid cells of δWDphag mice
LysM cre
δWD
δWD
X
Atg16L1fl
Atg16L1fl
50%
50%
δWDphag
LysM cre
Atg16L1fl
δWD
cre
Atg16L1fl
δWD
Atg16L1fl
δWD
Atg16L1fl
δWD
litter mate control
B
Atg16L1
654 bp
223
226
291 bp
290
291
Exon1
Exon2
3 4 5
6
7 8 9
10 11 12
13 14
15
16 17 18
δWD
654 bp
223
226
639 bp
290
291
stop
Exon1
Exon2
3 4 5
6
7 8 9
10 11 12
13 14
15
16 17 18
Atg16L1fl/fl
801 bp
223
LoxP LoxP
226
Exon1
Exon2
3 4 5
6
7 8 9
10 11 12
13 14
15
16 17 18
Atg16L1fl/fl LysMcre
253 bp
223
226
stop
Exon1
3 4 5
6
7 8 9
10 11 12
13 14
15
16 17 18
+
Exon 2

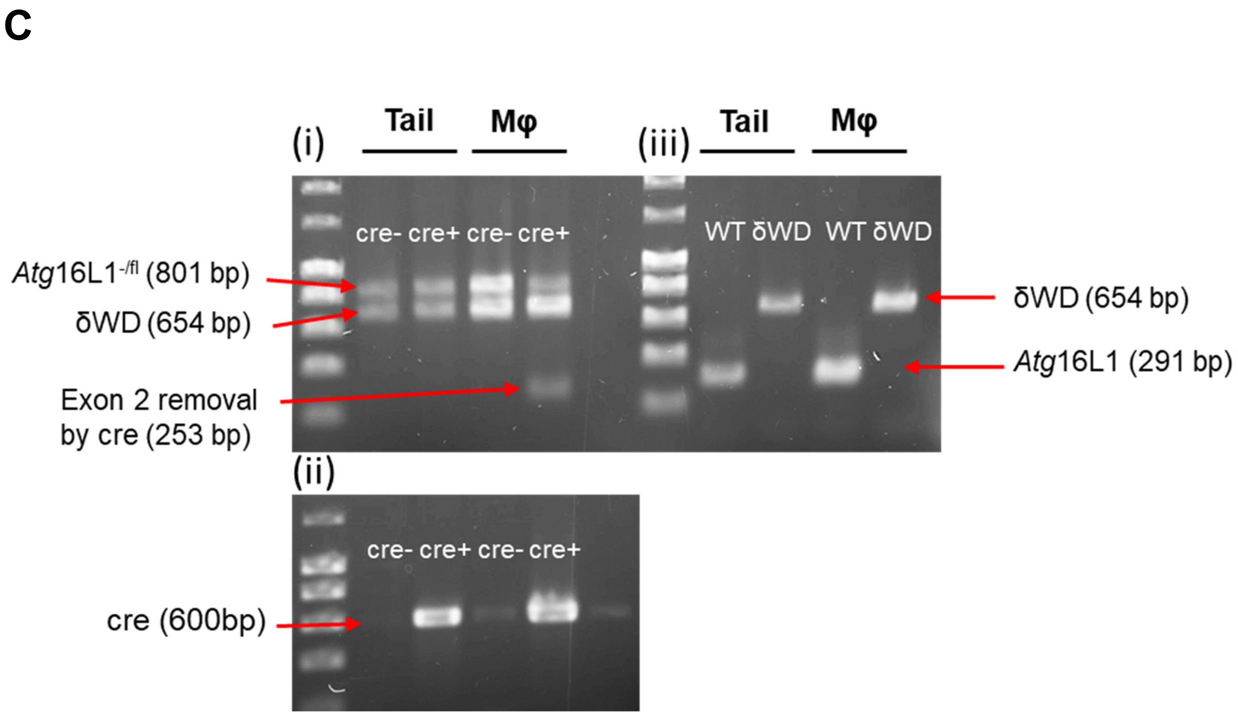
C
(i)
Tail
Mφ
cre- cre+ cre- cre+
Atg16L1-/fl (801 bp)
δWD (654 bp)
Exon 2 removal by cre (253 bp)
(iii)
Tail
Mφ
WT δWD WT δWD
δWD (654 bp)
Atg16L1 (291 bp)
(ii)
cre- cre+ cre- cre+
cre (600bp)

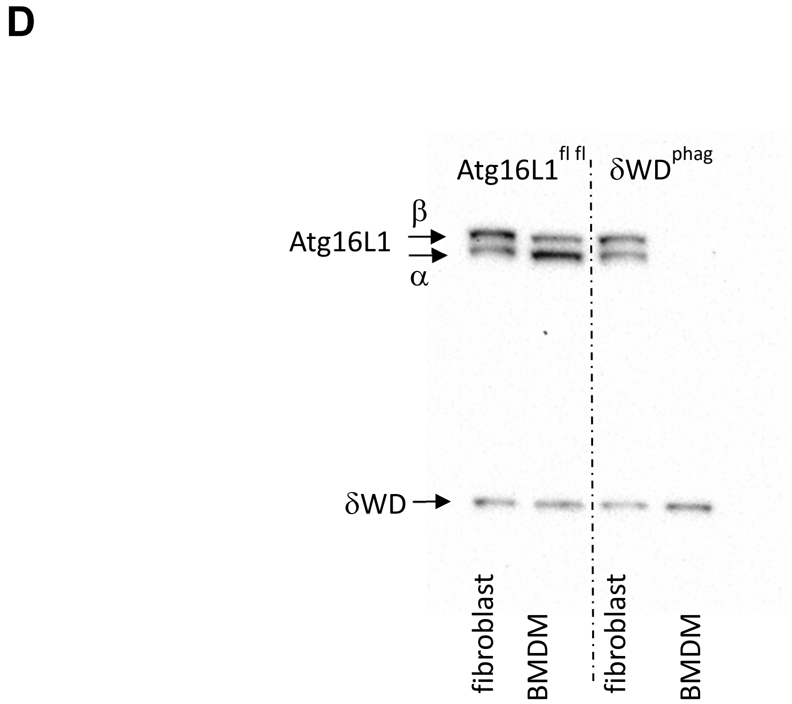
D
Atg16L1 fl fl
δWD phag
Atg16L1
β
α
δWD
fibroblast
BMDM
fibroblast
BMDM

E

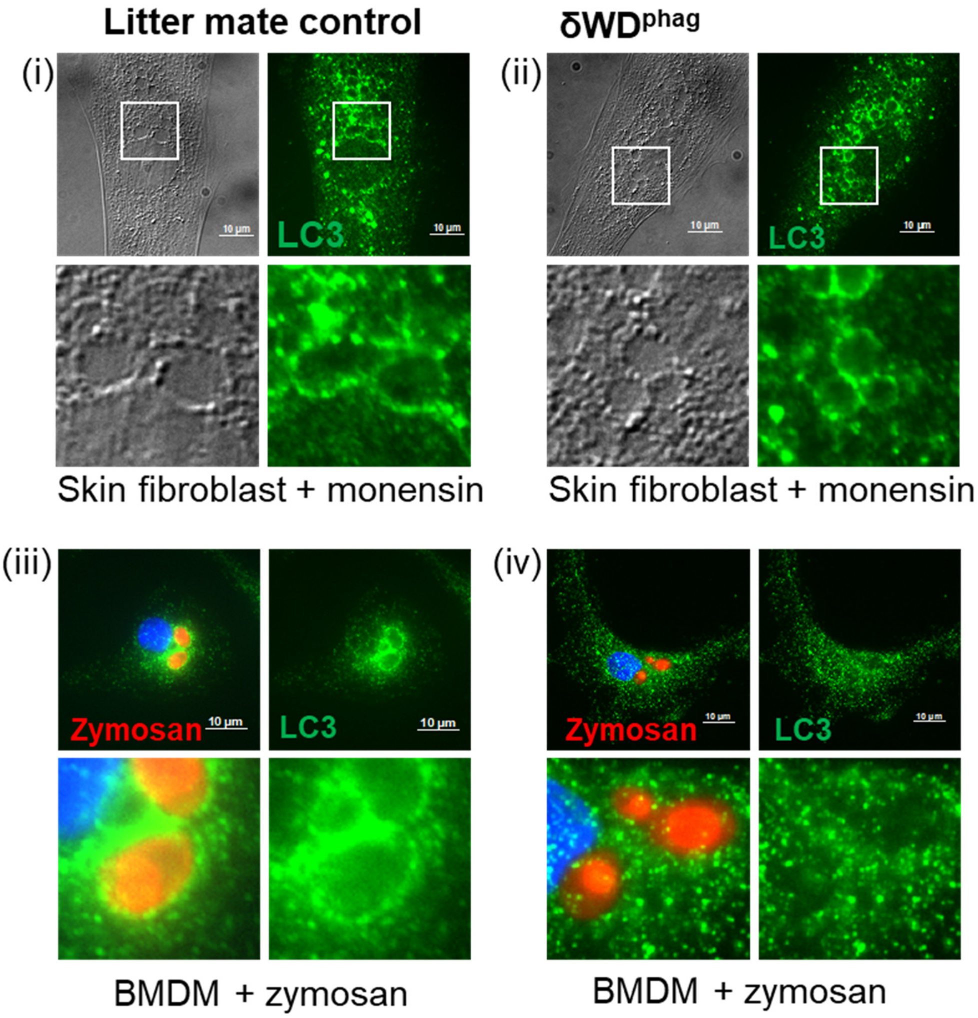

Fig. S7. Generation of δWD^{phag} mice

Panel A. ***Breeding strategy.*** Homozygous δWD mice carrying LysMcre were crossed with *Atg*16L1$^{fl/fl}$ mice. 50% of progeny are *Atg*16L1$^{fl/δWD}$ and carry LysMcre. Cre recombinase expressed in myeloid cells of these mice inactivates *Atg*16L1 by removing exon 2 from *Atg*16L1 (δWD^{phag}). The myeloid cells only express δWD. Cre recombinase is not expressed in non-myeloid tissues and *Atg*16L1 is preserved to power autophagy. 50% of progeny provide littermate controls because they lack LysMcre and preserve *Atg*16L1 in all tissues.

Panel B. ***Genome map and PCR primers for analysis of the Atg16L1 genotype***. Unmodified *Atg16*L1 is identified using primers flanking exon 2 (223, 226) and exon 6 (290 and 291). The δWD allele was generated by inserting a stop codon into exon 6 and this increases the size of the PCR product of exon 6 from 291 bp to 639 bp. In *Atg*16L1^{flfl} loxp sites flanking exon 2 in Atg16L1 increase the PCR product of exon 2 from 654 bp to 801 bp, while removal of exon 2 by cre recombinase reduces the PCR product of exon 2 from 801 bp to 253 bp.

Panel C. ***Genotyping δWD^{phag} mice.*** DNA extracted from mouse tail tissue or bone marrow derived macrophages (MΦ) was analysed by PCR. **(i).** Samples from δWD^{phag} mice (indicated by cre+) and littermate controls (cre-). The 253bp PCR product seen in macrophage DNA of cre+ δWD^{phag} strains indicates specific removal of exon 2 from *Atg*16L1 in myeloid cells. **(ii).** PCR primers verify presence of cre recombinase (cre+). iii). Genotyping of wild type and δWD strains showing predicted changes in size of PCR product from exon 6.

Panel D. Tissue specific expression of ATG16L1 and δWD. Skin fibroblasts and bone marrow derived macrophages (BMDM) isolated from *Atg*16L1δWD^{phag} mice (δWD^{phag}) and littermate controls were analysed by western blot. Skin fibrobalasts and BMDM from control mice lacking LysMcre (Atg16L1$^{fl/fl}$) express full length 70kDa α and β isoforms of ATG16L1 and the truncated δWD at 25kDa. δWD^{phag} mice express LysMcre indicated by the removal of full length ATG16L1 from BMDM but not skin fibroblasts.

Panel E. Functional analysis of δWD^{phag} mice

Panels (i) and (ii). Analysis of non-canonical autophagy/LC3 associated endocytosis in fibroblasts from δWD^{phag} mice. Skin fibroblasts isolated from *Atg*16L1δWD^{phag} mice (δWD^{phag}) and litter mate controls were incubated with monensin to induce LC3 associated endocytosis, fixed and immunostained for LC3. Fibroblasts from δWD^{phag} mice are able to recruit LC3 (green) to swollen endo-lysosome compartments in a similar way to those from littermate control mice.

Panels (iii) and (iv). Analysis of non-canonical autophagy/LAP in BMDM from δWD^{phag} mice. BMDMs isolated from *Atg*16L1δWD^{phag} mice (δWD^{phag}) and litter mate controls were incubated with zymosan for 30 min, fixed and immunostained for LC3. BMDMs from δWD^{phag} mice are unable to recruit LC3 (green) to phagosomes containing zymosan (red).

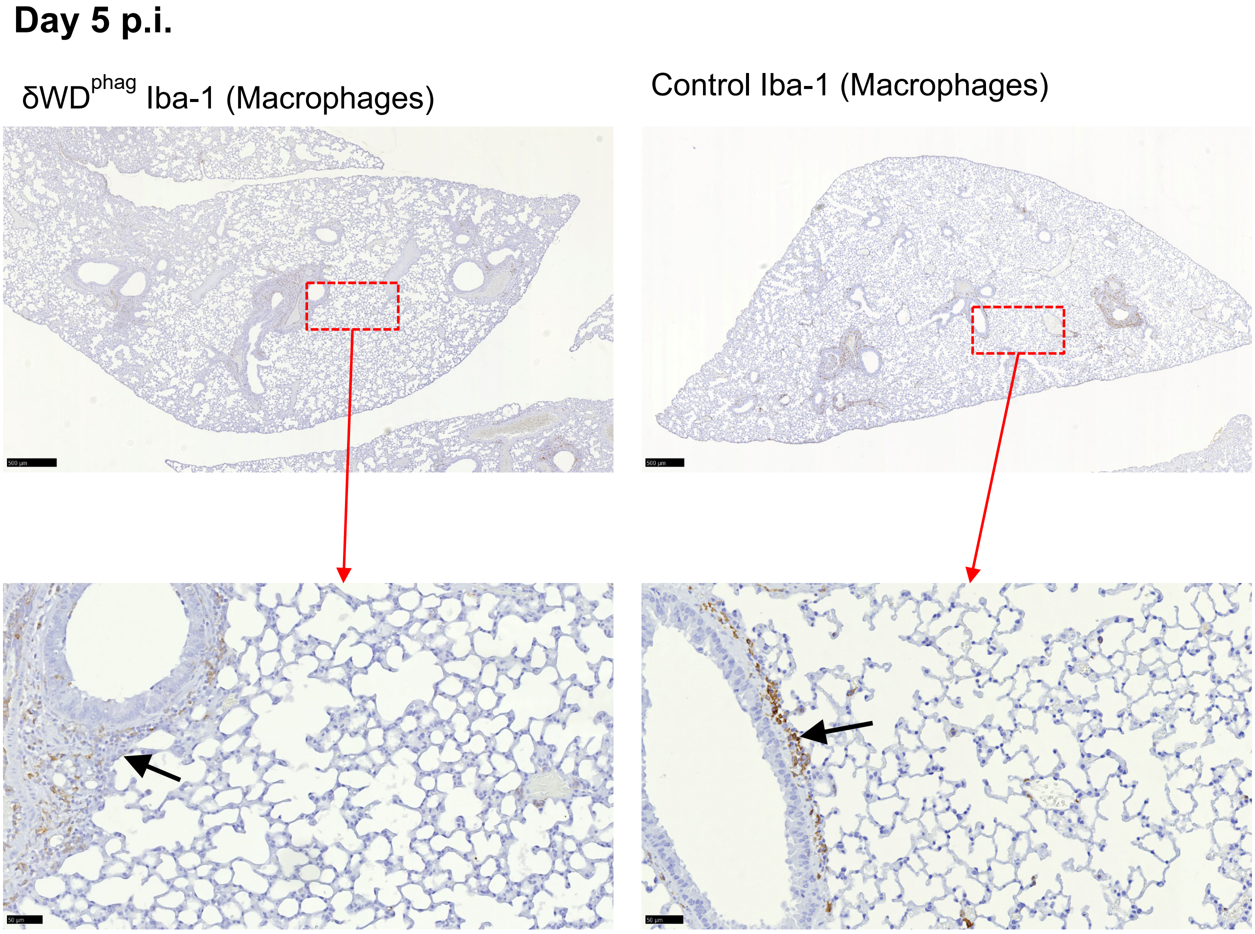

Fig. S8. Mice deficient in non-canonical autophagy/LAP in phagocytes control IAV infection and do not show increased lung inflammation

δWD^{phag} that are deficient in non-canonical autophagy in phagocytes and littermate control mice were infected i.n. with 10^3 pfu IAV X31. Lung tissues were harvested at 5 d p.i. Macrophages were detected by IH using anti-Iba-1, visualized with DAB and counter-stained with hematoxylin. Scale bars represent 500 µm (upper panels) and 50 µm (lower panels). Micrographs of representative areas from lungs of six mice are shown. Both δWD^{phag} and control mice show little inflammatory response in the parenchyma and mild, macrophage-rich peri-bronchiolar infiltration (black arrows).